

Frequency response analysis of the in-vivo human spine
by Stephen Walter Radons

A thesis submitted in partial fulfillment of the requirements for the degree of MASTER OF SCIENCE in MECHANICAL ENGINEERING
Montana State University
© Copyright by Stephen Walter Radons (1978)

Abstract:
In this study, a finite element model of the human spine is presented. The intent of this research is to investigate the possibility of using the frequency response analysis technique as a diagnostic tool for determining the success of spinal fusions.

Two boundary conditions are studied such that the actual boundary condition is assumed to be between those used. One boundary condition has the spine pinned at the sacrum and the other boundary condition has the spine fixed to the sacrum. An analytical solution is obtained approximating the normal spine, the fused scoliotic spine, and the fused scoliotic spine with a Harrigan rod implant.

A comparison to experimental results is made for the cases listed above as well as the different boundary conditions used.

The results indicate that the use of the natural frequencies of the spine as a diagnostic tool have major experimental and analytical problems associated with them. The possible use of mode shape changes when spinal fusions are performed may have diagnostic potential but the technique needs added experimental and analytical research before a definite decision on this method can be made. The indication of dampening calls for an extended analysis that includes the dampening effects.

STATEMENT OF PERMISSION TO COPY

In presenting this thesis in partial fulfillment of the requirements for an advanced degree at Montana State University, I agree that the Library shall make it freely available for inspection. I further agree that permission for extensive copying of this thesis for scholarly purposes may be granted by my major professor, or, in his absence, by the Director of Libraries. It is understood that any copying or publication of this thesis for financial gain shall not be allowed without my written permission.

Signature Stephen W. Radons

Date 10/25/78

FREQUENCY RESPONSE ANALYSIS OF THE IN-VIVO HUMAN SPINE

by

STEPHEN WALTER RADONS

A thesis submitted in partial fulfillment
of the requirements for the degree

of

MASTER OF SCIENCE

in

MECHANICAL ENGINEERING

Approved:

Dennis O. Blackketter
Chairperson, Graduate Committee

Thomas C. Pedersen
Head, Major Department

Henry L. Parsons
Graduate Dean

MONTANA STATE UNIVERSITY
Bozeman, Montana

October, 1978

ACKNOWLEDGEMENT

The author would like to express his appreciation to Dr. Dennis O. Blackketter for his assistance during the period of this study. Special thanks goes to Dr. John Jurist for the permission to use his experimental results.

TABLE OF CONTENTS

	Page
VITA	ii
ACKNOWLEDGEMENTS	iii
LIST OF TABLES	v
LIST OF FIGURES	vi
ABSTRACT	ix
CHAPTER I. INTRODUCTION	1
CHAPTER II. LITERATURE REVIEW	3
CHAPTER III. THE HUMAN SPINE	6
CHAPTER IV. MODELING THE SPINE SYSTEM	21
CHAPTER V. FREQUENCY RESPONSE	38
CHAPTER VI. RESULTS	40
CHAPTER VII. DISCUSSION	58
APPENDIX I. DEVELOPMENT OF FINITE ELEMENT MATRICES	62
APPENDIX II. ANTHROPOMETRIC DATA	83
APPENDIX III. PROBLEMS ARISING USING THE SWEEPING MATRIX TECHNIQUE SOLUTION	92
REFERENCES	93

LIST OF TABLES

	Page
TABLE 3-1.--Muscles of the Back	15
TABLE 6-1.--Changes in Analytic Vertebral Natural Frequencies due to Spinal Fusion	53
TABLE II-1.--Global Coordinates	83
TABLE II-2.--Global Coordinates of Curvature for Rib Elements .	85
TABLE II-3.--Intervertebral Disc Data Used	86
TABLE II-4.--Vertebral Dimensions	88
TABLE II-5.--Spring Level Arm Lengths in Inches	89
TABLE II-6.--Vertebral Data	90
TABLE II-7.--Rib Data	90
TABLE II-8.--Rib Section Data	91

LIST OF FIGURES

Page

3-1.--The vertebral column 7

3-2.--The structure of the vertebrae 9

3-3.-- Atlas, cranial view 10

3-4.--Axix, ventral view and dorsal view 11

3-5.--Schematic of intervertebral disc 13

3-6.--Superficial muscles of the back 17

3-7.--Deep muscles of the back 18

3-8.--Costovertebral articulations 19

4-1.--Modeling concepts of vertebral column 21

4-2.--Rib plane configuration 23

4-3.--Schematic of model 24

4-4.--Assumed X_2 displacements 31

4-5.--Elemental nomenclature 36

6-1a.-First bending mode of the spine 41

6-1b.-Second bending mode of the spine 41

6-1c.-Third bending mode of the spine 42

6-1d.-First bending mode of the ribs 42

6-1e.-Fourth bending mode of the spine 43

6-1f.-Second bending mode of the ribs 43

6-2.--Change of first natural frequency of the spine 45

6-3.--Change in second and third natural frequencies of the spine 46

LIST OF FIGURES (cont.)

Page

6-4.--Change in fourth natural frequency of the spine 47

6-5.--Change in first and second natural frequencies of the ribs 48

6-6.--Change in first vertebral frequency 49

6-7.--Change in vertebral frequencies two and three 50

6-8.--Experimental frequency response of 22-year old male . . . 51

6-9.--Analytical frequency response (ρ) case 51

6-10a. Motion associated with third natural frequency of normal spine 54

6-10b. Motion associated with third natural frequency of fused spine 54

6-10c. Motion associated with second natural frequency of fused spine with added Harrigan rod 54

6-11.- Analytical frequency response plot for the fused spine with Harrigan rod implent 55

6-12.- Experimental frequency response plot for scoliotic spine 56

I-1.--Global and elemental coordinate systems 62

I-2.--Elongation of spring elements 63

I-3.--Head spring 70

I-4.--Rib spring 71

I-5.--Vertebral element 72

I-6.--Sacral mass 75

I-7.--Straight beam element 76

LIST OF FIGURES (cont.)

Page

I-8.--Curved beam element 79

II-1.-Second cervical measurements 87

II-2.-Vertebrae and intervertebral disc measurements 87

II-3.-Lever arms used for the various ligaments, muscles, and fusions 88

II-4.-Rib Geometry 89

ABSTRACT

In this study, a finite element model of the human spine is presented. The intent of this research is to investigate the possibility of using the frequency response analysis technique as a diagnostic tool for determining the success of spinal fusions.

Two boundary conditions are studied such that the actual boundary condition is assumed to be between those used. One boundary condition has the spine pinned at the sacrum and the other boundary condition has the spine fixed to the sacrum. An analytical solution is obtained approximating the normal spine, the fused scoliotic spine, and the fused scoliotic spine with a Harrigan rod implant.

A comparison to experimental results is made for the cases listed above as well as the different boundary conditions used.

The results indicate that the use of the natural frequencies of the spine as a diagnostic tool have major experimental and analytical problems associated with them. The possible use of mode shape changes when spinal fusions are performed may have diagnostic potential but the technique needs added experimental and analytical research before a definite decision on this method can be made. The indication of dampening calls for an extended analysis that includes the dampening effects.

CHAPTER I

INTRODUCTION

Several investigations into the response of the human spine to an externally applied harmonic excitation have been carried out. These investigations indicate that several natural frequencies, or bending modes, exist for the spine in the sagittal plane when it is excited harmonically through the frequency range of 30 to 500 hertz. The purpose of this research is to develop an analytical vibrations model of the human spine that can adequately simulate the experimental frequency response. The proposed use of the model is to determine the healing rate of the scoliotic spine by comparing frequency response of the spine after a corrective procedure with the anticipated frequency response predicted by the model.

The experimental frequency response plots in this study were obtained from Dr. John Jurist, of the Deaconess Hospital in Billings, Montana. These frequency response plots were acquired by placing a low amplitude harmonic exciter on a spinous process of one vertebra and a transducer for output on a different vertebral spinous process. The frequency response plots have peak amplitudes where the systems natural frequencies occur. The band width of these peaks indicates the damping inherent to the system. A model that accurately simulates the experimental frequency response can be used to predict the response when physical changes in the spine are encountered. This may be useful as a tool for determining rheological parameters of in-vivo human bone and

tissue. Previously, in-vivo properties were obtained from, or extrapolated from, in-vitro studies resulting in somewhat inaccurate values since tissue properties change within a matter of minutes after death.

The model used in describing the spine utilizes the finite element technique. The spine is modeled as 23 rigid bodies representing the vertebrae, 23 elastic beam elements representing the intervertebral discs, and 30 curved elastic beam elements representing the ribs. Four linear springs join adjacent vertebrae representing the various ligaments and muscles associated with the spine as well as the possible fusion tissue used to stiffen the spine. The fusion material is usually calcified bone used to stiffen the scoliotic spine. The head mass is included and rests on a spring representing flesh. The ribs are likewise supported on the frontal ends by springs representing the collagenous connection to the sternum. All along the vertebral column, an elastic substrate is used to represent internal flesh. Two cases are studied; one with the spine pivoted about the sacral connection and one with the spine cantilevered to the sacrum.

Due to the large computer storage and time required in solving the resulting 270 and 269 degree of freedom systems, a reduction of coordinate scheme is used to reduce the global coordinates to 16 generalized coordinates. Validity of the model is indicated by matching natural frequencies of the model to those obtained experimentally from a 22 year old male.

CHAPTER II

LITERATURE REVIEW

Most previous work analyzing the spine as a mechanical system has been affiliated with high acceleration response. These studies were triggered by the large number of spinal injuries encountered with high acceleration ejections from aircraft.

The first models of the spine were simple lumped mass systems. Latham [2] modeled the spine as a weightless spring supporting a mass. Other similar models were developed using various means to determine the spring constant of the spine. All of these were single degree of freedom models which did not account for the change of curvature of the spine in the sagittal plane or the resulting stresses due to this change. To study sagittal plane effects, Hess and Lombard [3] modeled the spine as an elastic beam. Terry and Roberts [4] added viscoelastic effects to the Hess-Lombard model. The results of these earlier models indicated the need for a discrete model composed of mass-spring-dashpot elements representing each of the intervertebral discs and vertebrae. The necessity for a discrete model required an extensive experimental investigation of the rheological properties of the vertebrae and intervertebral discs. This investigation was first accomplished by Orne and Liu [5].

Andriacchi, et. al. [6] developed a three-dimensional mathematical model of the spine along with the interacting ribs. The model incorporated anatomical features such as sagittal plane curves, the complex geometric shape of each vertebra and rib, and level to level variations

in stiffness of connective tissue. The model did not include viscoelastic effects or the upper cervical spine and head mass.

Previous vibration studies of biological systems have been limited. Jurist [7] proposed using the measurement of the resonant frequency of the ulna and other long bones as a means of disease detection or as a monitor of fracture healing. He described effects of experimental procedures, geometry, positioning, and muscle tension associated with this technique. He also discussed the reproducibility of experimental results.

Matz [8] set up an experiment similar to Jurist's and carried out a statistical analysis of a large sample of humans. He vibrated the forearm transversely at a low amplitude over a frequency range of 80 to 600 hertz. Four factors, bone size, arm length, muscle development, and fleshiness, were correlated with the first resonant frequency. Mozer [9] determined the effect of stiffness on the first natural frequency of the forearm and Harrigan [10] refined the development of equipment used in determining the dynamic response of a forearm.

Garner and Blackketter [1] extended the analysis of the forearm by developing a finite element model. A steady-state response to harmonic excitation was obtained for the three-dimensional, viscoelastic model with results in good agreement to those obtained by Matz.

Jurist and Blackketter [11] discussed possible uses of the frequency response method in the monitoring of long bone fracture healing

rates, rates of osteoporosis (bone mineral content loss), and stiffening rates of the scoliotic spine.

Adelsbach [12] modeled the spine as a series of rigid bodies (vertebrae) connected by viscoelastic beam elements (intervetrabral discs) with a pinned boundary at the bottom of the lumbar spine and a rolling support at the upper cervical vertebra. The head mass and ribs were ignored in this analysis. His results show the first natural frequency of the spine to be near 40 hertz.

CHAPTER III

THE HUMAN SPINE

In order to model the human spine accurately, information on the makeup of the spine and its association with related parts of the body is necessary.

The Vertebral Column

The vertebral column (Figure 3-1) consists of 24 vertebrae held in position by strong ligaments, muscles, and by the interlocking nature of their articulations. All vertebrae have basically the same structural pattern with slight variations in size and in some of the processes. The vertebrae are classified in groups in which there are seven cervical, twelve thoracic, five lumbar, five sacral, and four coccygeal vertebrae. The sacral and coccygeal vertebrae usually fuse into one sacrum and one coccyx.

The normal vertebral column exhibits four curvatures in the lateral view; two curving frontally, known as primary curves, and two curving posteriorly, known as secondary curves. The primary curves are located in the thoracic and sacral regions.

Abnormalities in curvatures are common. An excessive thoracic curvature is acknowledged as kyphosis (known as hunchback). A pronounced lumbar curvature is recognized as lordosis and a lateral curvature is known as scoliosis.

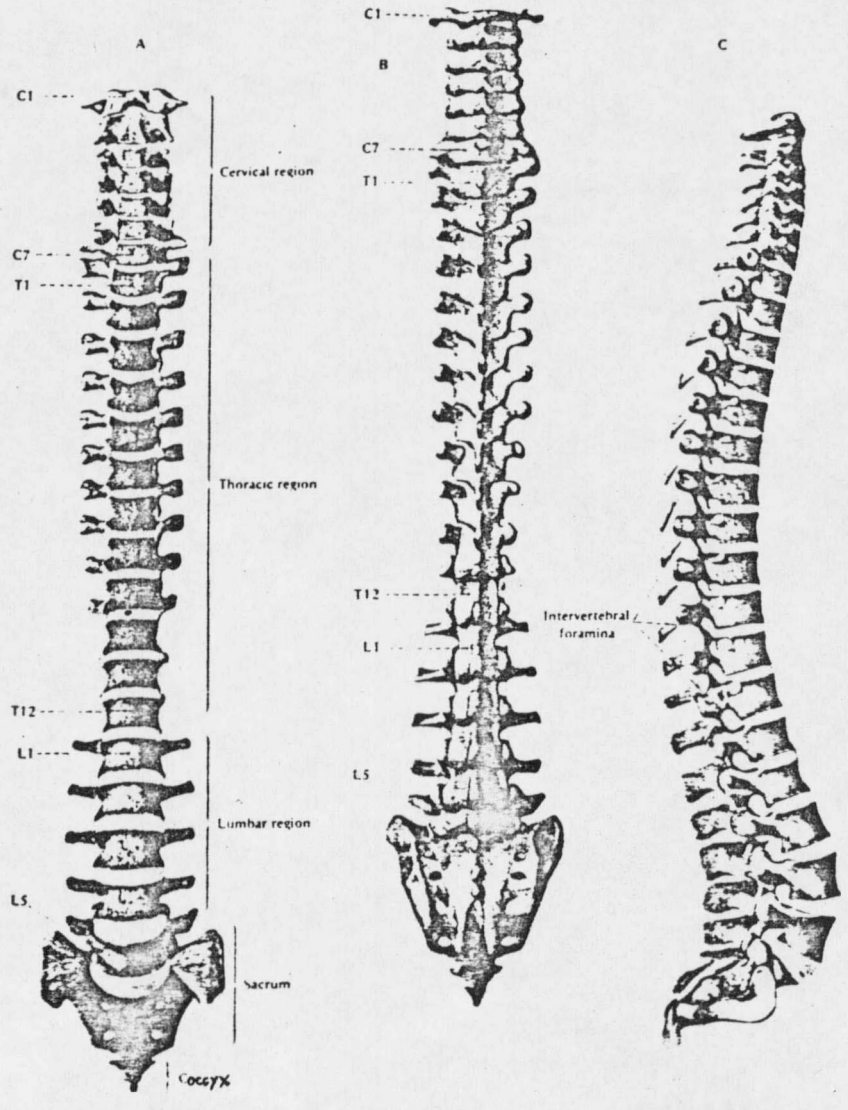


Figure 3-1.--The Vertebral Column. A: Anterior view. B: Posterior view. C: Lateral view. Source: B. R. Landau, Essential Human Anatomy and Physiology.

A typical vertebra (Figure 3-2) consists of a body with a vertebral arch attached to its posterior surface. This arch encloses an opening, the vertebral foramen, which contains the spinal cord. From the arch arise four processes for articulations and three processes primarily for attachments of ligaments and muscles. Those associated with articulation are the paired superior and inferior articular processes. The three remaining processes are the paired transverse processes which extend laterally and the single spinous process which protrudes posteriorly at an angle from the arch. Each body is connected to the adjacent vertebrae through fibrocartilage discs called intervertebral discs. The vertebral bodies increase in size as one proceeds from the top of the spine to the bottom.

All vertebrae in the spine are basically the same as that depicted by Figure 3-2 with the exception of the first and second cervical vertebrae. The first cervical (Figure 3-3), the Atlas, has no body. It is essentially a ring with two lateral masses. The superior articular processes are modified to a pair of large concave articular facets which the head rides on. The second cervical, the Axis (Figure 3-4) has a tooth-like process, the dens, which protrudes upward from its body. Ligaments hold the dens in place behind the anterior arch of the atlas such that it serves as the body of the atlas.

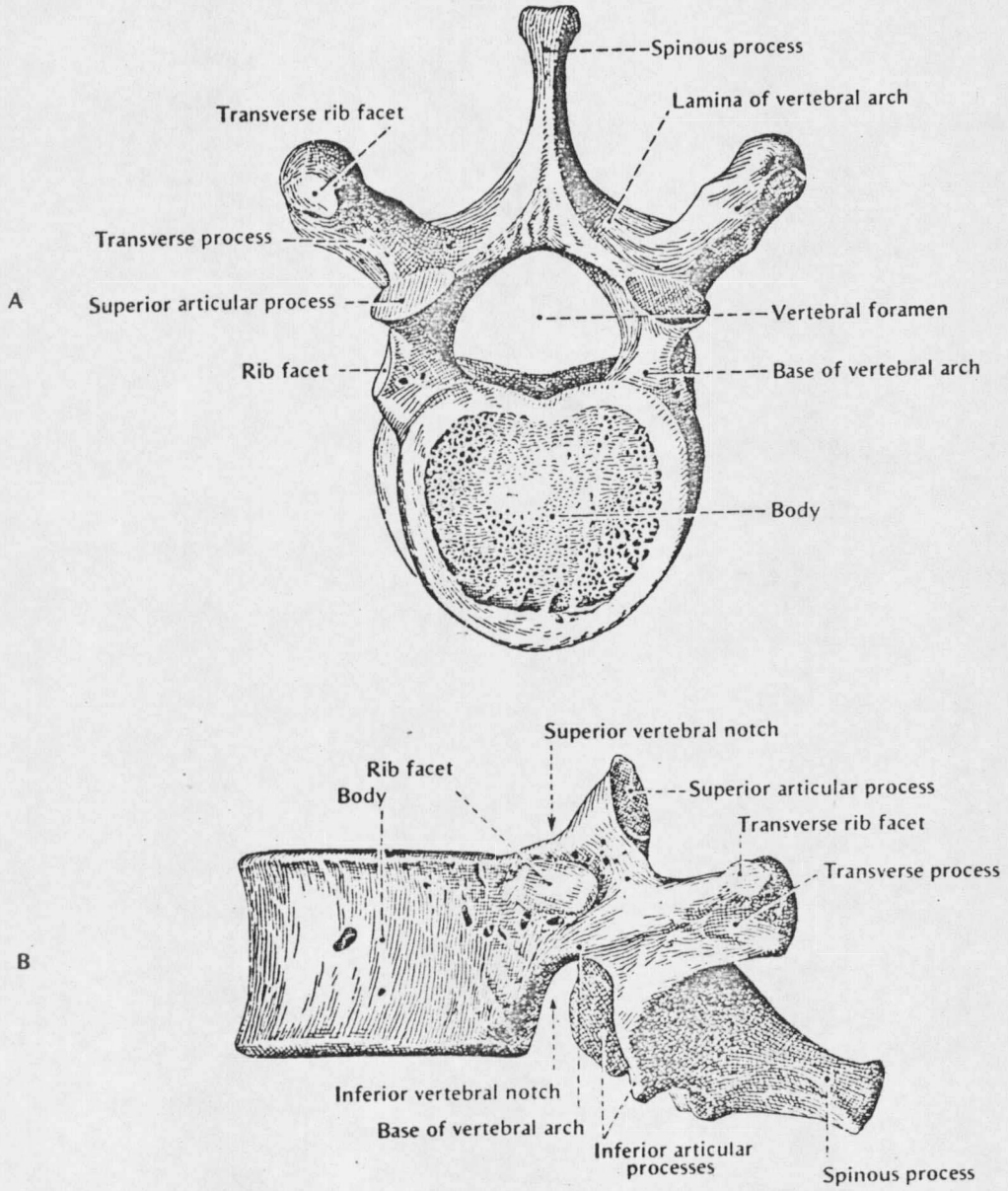


Figure 3-2.--The Structure of the Vertebrae, Illustrated by a typical thoracic vertebra. Source: B. R. Landau, Essential Human Anatomy and Physiology.

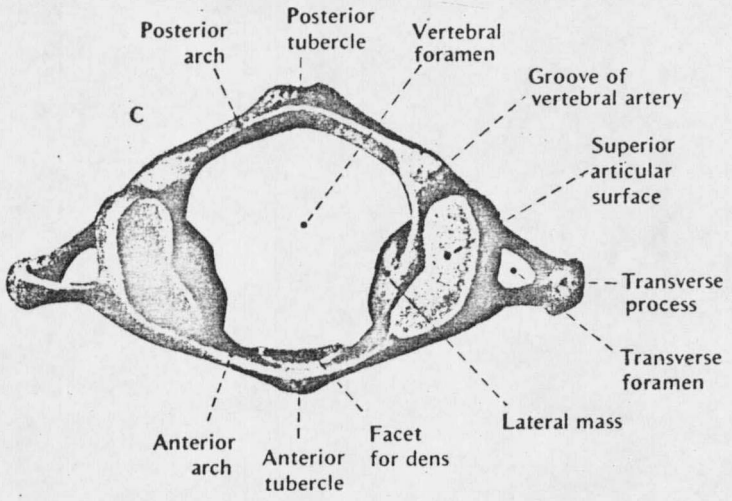


Figure 3-3.--Atlas, cranial view. Source: B. R. Landau, Essential Human Anatomy and Physiology.

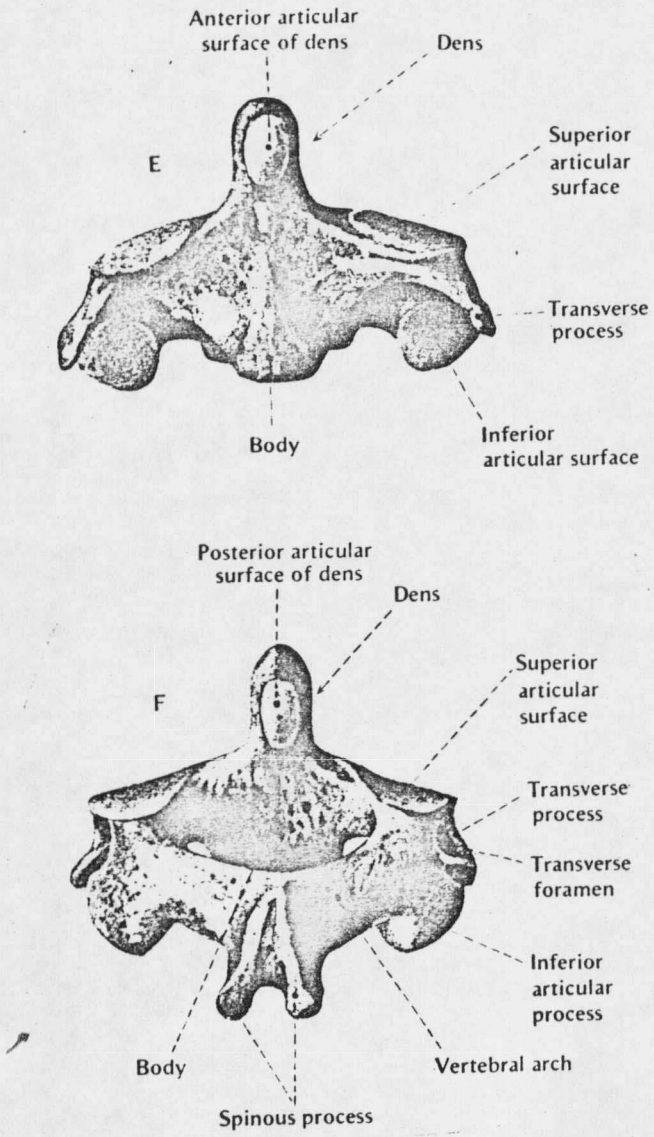


Figure 3-4.--Axis, ventral view and dorsal view. Source: B. R. Landau, Essential Human Anatomy and Physiology.

Bone is a connective tissue in which the intercellular substance consists of mineral deposits composed mainly of inorganic salts of calcium and phosphate complex. The cells and fibers are largely protein. Thus, bone is hard and rigid due to the minerals and tough due to the cells and fibers. The body of the vertebra is composed of an outer ring of dense material called compact bone, its center filled with cancallous bone. The articular surfaces and processes are basically shells of compact bone with cancellous material for cores much the same as the body. There is no marrow cavity in the vertebra.

The intervertebral disc is a fibrocartilage pad (Figure 3-5). Fibrocartilage is composed of collagen fibers and reinforcing ligaments which together assure strong union between bones. Collagen fibers are composed of fibers which are strong and inflexible. A gelatin type substance is intermingled with these fibers. Ligaments are much the same in composition. The intervertebral discs must support weight and absorb shock; therefore, its structure includes a mass of fibrogelatinous pulp (nucleus pulposus) at the core as a shock absorber. Around the core are wrapped concentric rings of fibers (annulus fibrosus). Under sudden seyere pressure, the nucleus pulposus may break through the annulus fibrosus and cause pressure on nerves or may burst through into the body of the vertebra. The intervertebral disc is much more flexible than the vertebra and the vertebra is virtually a rigid body relative to the intervertebral disc.

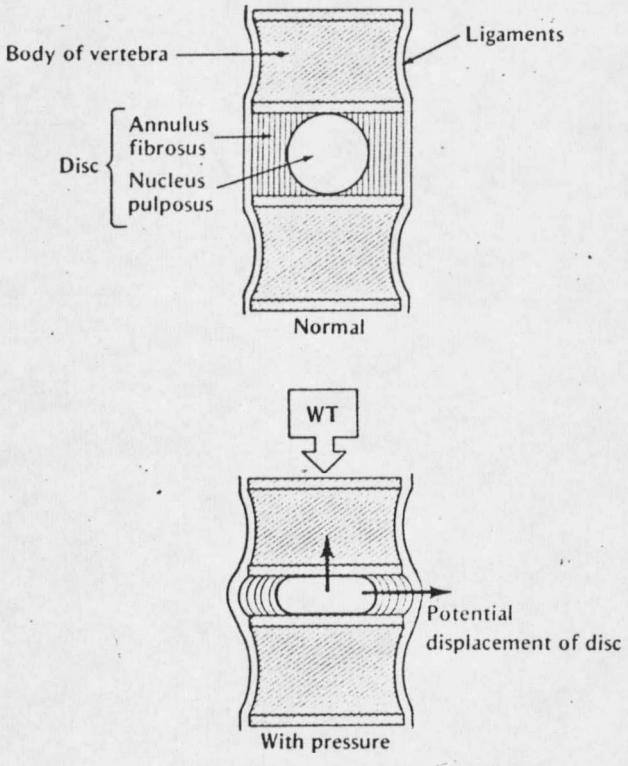


Figure 3-5.--Schematic of intervertebral disc. Source: B. R. Landau, Essential Human Anatomy and Physiology.

Ligaments, Muscles, and Connective Tissue

In addition to the intervertebral discs, the vertebrae are connected by several muscles and ligaments. The posterior vertebral muscles are divided into two groups referred to as superficial and deep muscles. These muscles are all located below the massive back muscles associated with the upper trunk. The superficial muscles insert several segments above their origins and act over several joints while the deep muscles

generally insert on the segments directly above their origins. Table 3-1 lists the muscles associated with the spine and their functions. Figure 3-6 shows the superficial muscles of the back and Figure 3-7 shows the deep muscles of the back.

The ligaments which connect adjacent vertebrae are shown in Figure 3-8. The intertransverse ligaments firmly bond the transverse processes of adjacent vertebrae together. The supraspinous ligament does the same for the spinous processes of adjacent vertebrae. A collagen tissue (not shown in Figure 3-8) connects the inferior and superior processes of adjacent vertebrae.

Ribs

The ribs articulate posteriorly with the twelve thoracic vertebrae The first seven ribs attach to the sternum through the costal cartilages. The next three are attached to the cartilage of the rib above it and are thus indirectly attached to the sternum. The final two ribs have no anterior articulation and are called floating ribs. Each rib has a round head that connects to the rib facets on the bodies of two vertebrae and a tubercle that connects with the rib facet on the transverse process of one of the vertebrae. The connective tissue is collagen and though the ribs move with their respective vertebrae, they are somewhat free to rotate about their connection points like ball and socket joints.

TABLE 3-1

Muscle	Origin	Insertion	Action
Superficial muscles of the back			
Splenius capitis	lower half of ligamentum nuche and transverse processes of seventh cervical and first four thoracic vertebrae	mastoid process and occipital bone	singly--abducts and rotates both--extends head and cervical region
cervicis	spinous process of third to sixth thoracic vertebrae	transverse processes of first three cervical vertebrae	
Erector spinal			
iliocostalis lumborum dorsi cervicis	laterally--angle of ribs and or pelvic girdle	angle of rib, or cervical vertebrae six segments above	extends vertebral column
longissimus dorsi cervicis capitis	medially--transverse processes of lumbar, thoracic, and cervical vertebrae	transverse processes of vertebrae six segments above	all extend and abduct the vertebral column, but only capitis acts on the head
spinalis dorsi cervicis	medially--spinous processes of thoracic and lowest cervical vertebrae	spinous processes six segments above	extends vertebral column

TABLE 3-1 Continued

Muscle	Origin	Insertion	Action
Deep muscles of the back			
Semispinalis dorsi cervicis capitis	transverse processes of thoracic and seventh cervical vertebrae	spinous processes six segments above and occipital bone (capitis)	extends and rotates vertebral column and head (capitis)
Multifidus	pelvic girdle, lumbar vertebrae, transverse processes of thoracic and lower cervical vertebrae	spinous processes three segments above	extends vertebral column; each side may abduct and rotate
Rotatores	transverse processes of all vertebrae	spinous process of vertebrae above	extends and rotates vertebral column
Interspinales	spinous processes, especially in cervical and lumbar regions	spinous process of vertebrae above	extends
Intertransversarii	transverse rpocesses, especially lumbar and cervical regions	transverse processes of vertebrae above	extends and abducts

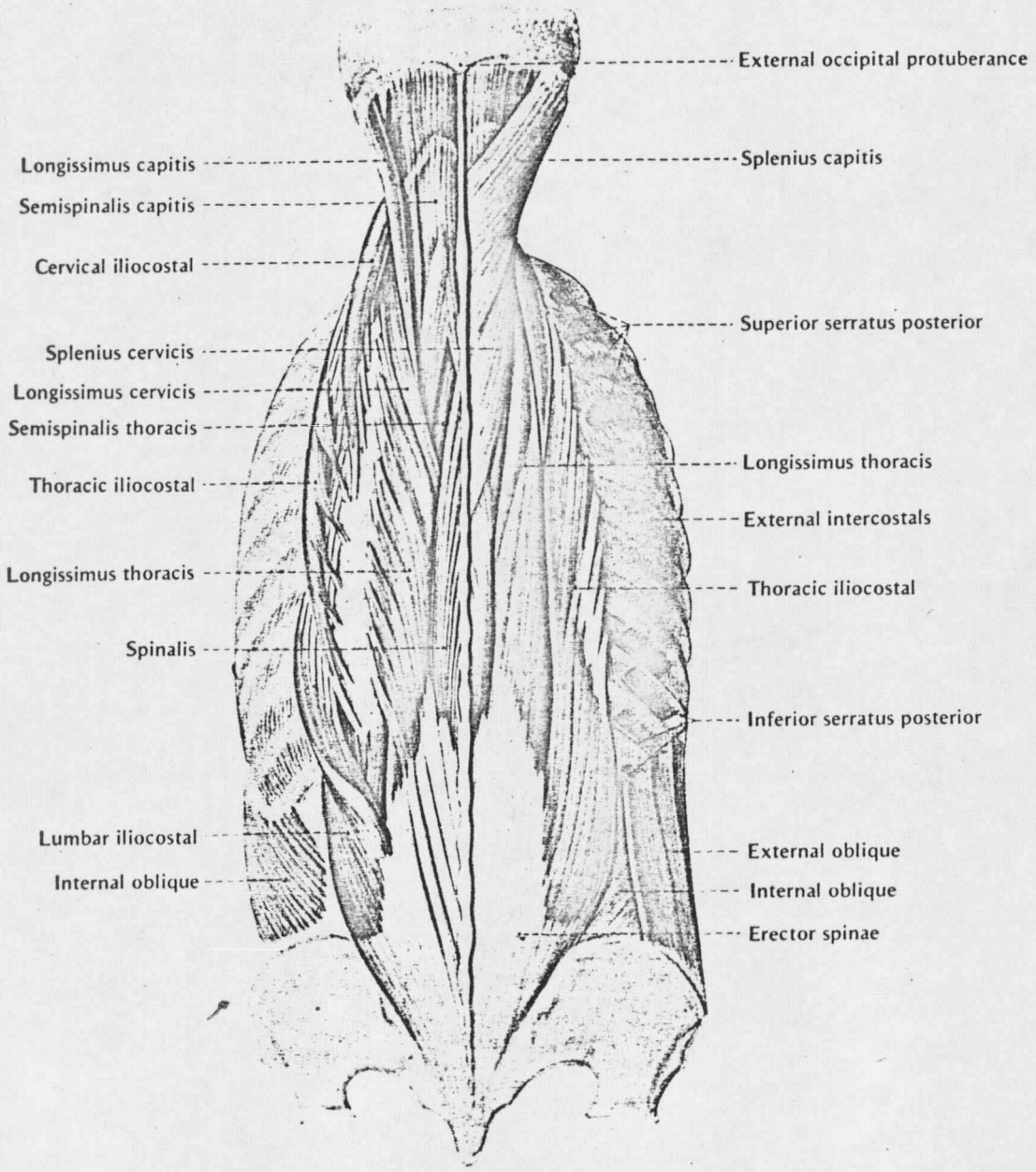


Figure 3-6.--Superficial muscles of the back. Source: B. R. Landau, Essential Human Anatomy and Physiology.

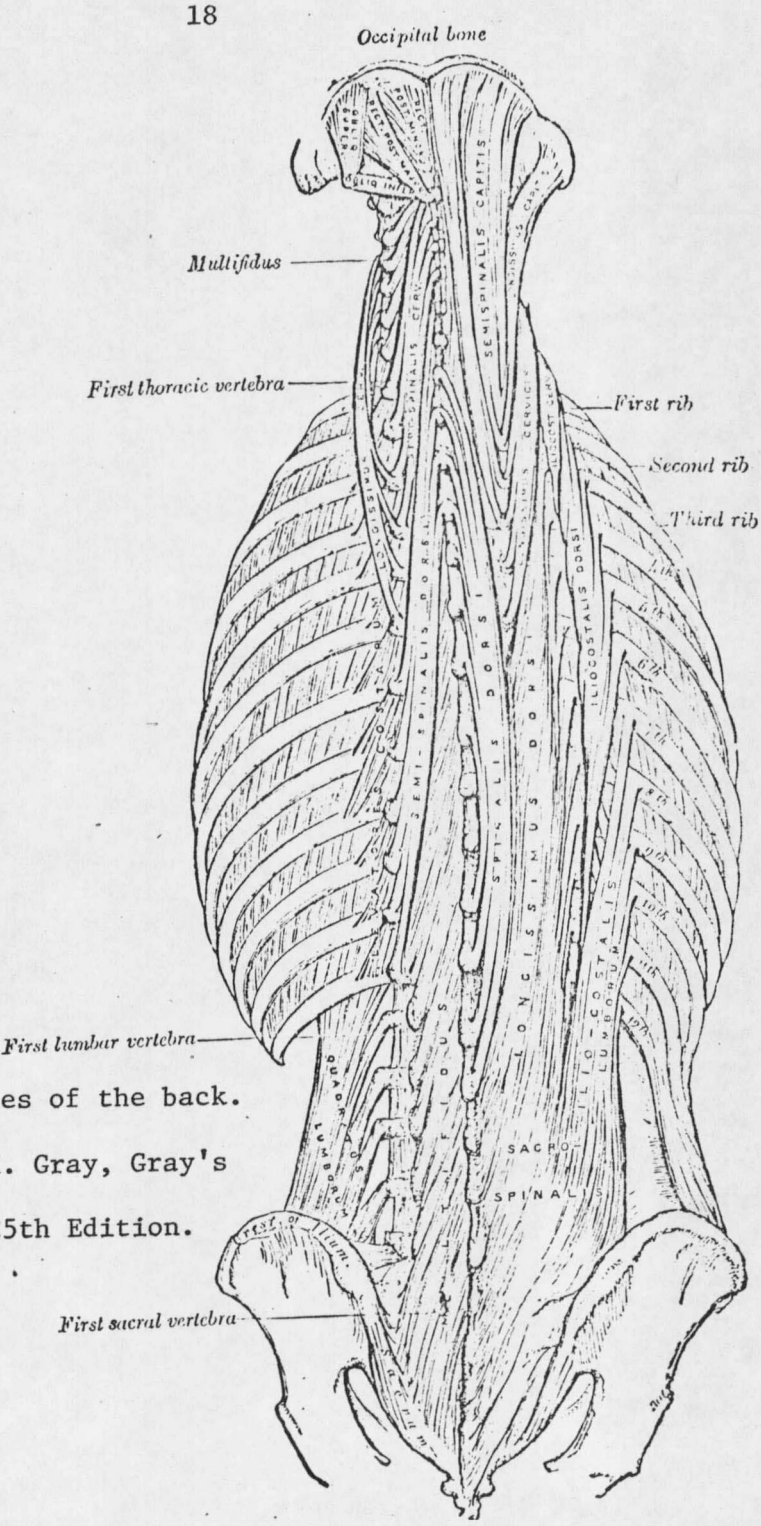


Figure 3-7.--Deep muscles of the back.

Source: H. Gray, Gray's Anatomy, 25th Edition.

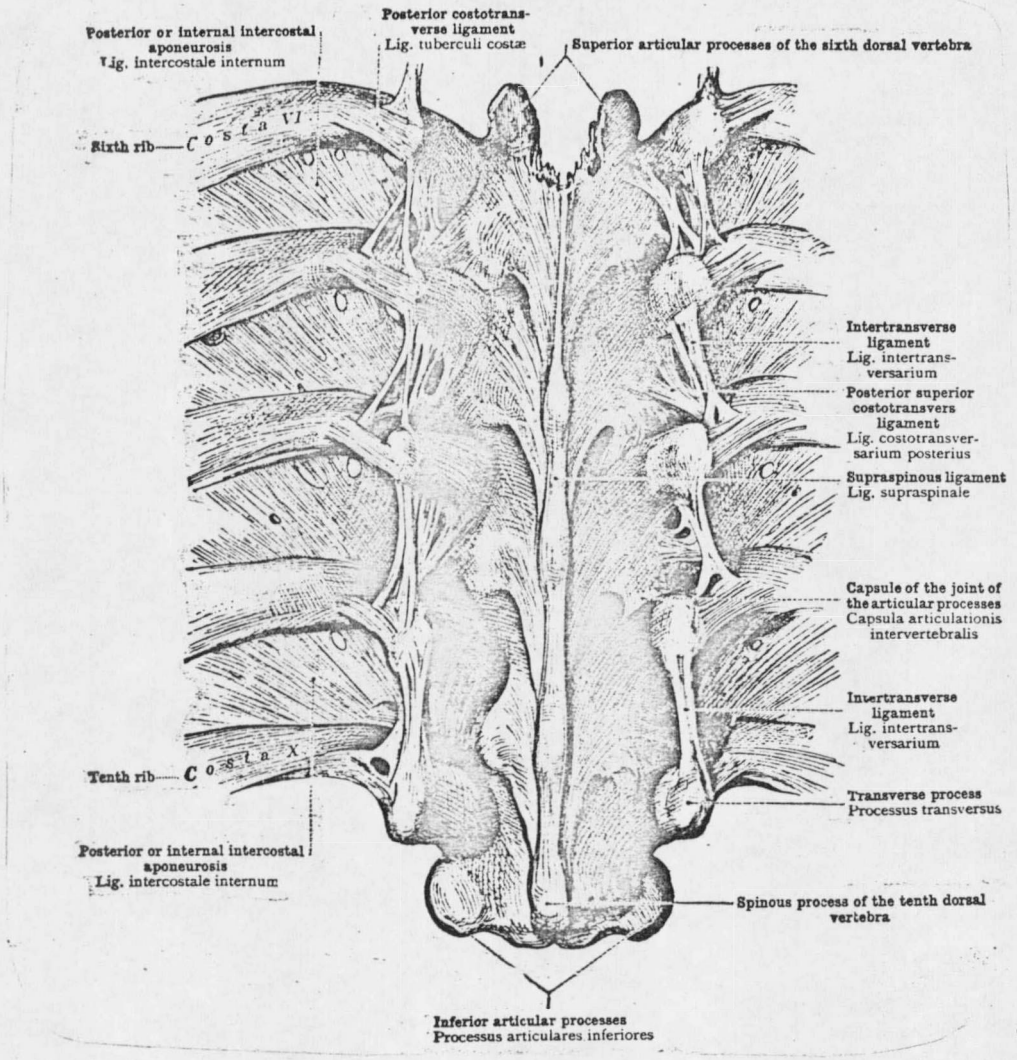


Figure 3-8.--Costovertebral articulations. Source: C. Toldt, M.D., An Atlas of Human Anatomy, Vol. 1, Second Edition.

Other Considerations

On the anterior side of the vertebrae lie several muscles and the internal organs of the human body. The digestive organs lie in front of the lumbar and middle to lower thoracic regions. The lungs lie in front of the upper thoracic region. Though these organs are very soft, they do constrain somewhat the position and movement of the spine.

Other bones are connected indirectly to the spine through attached bones such as the scapula (shoulder blade), clavicle (collar bone), and illium (pelvis). Assumptions were made to limit model complexity introduced by these bones.

CHAPTER IV

MODELING THE SPINE SYSTEM

The model was constructed such that consideration of medical benefits of geometric changes, material property variations, bone fusions, and Harrigan rod implants could be determined.

The Model

The spine was modeled as a series of rigid bodies (vertebrae) connected by finite beam elements (intervertebral discs) and four springs representing various ligaments and muscles. This is shown schematically in Figure 4-1 below.

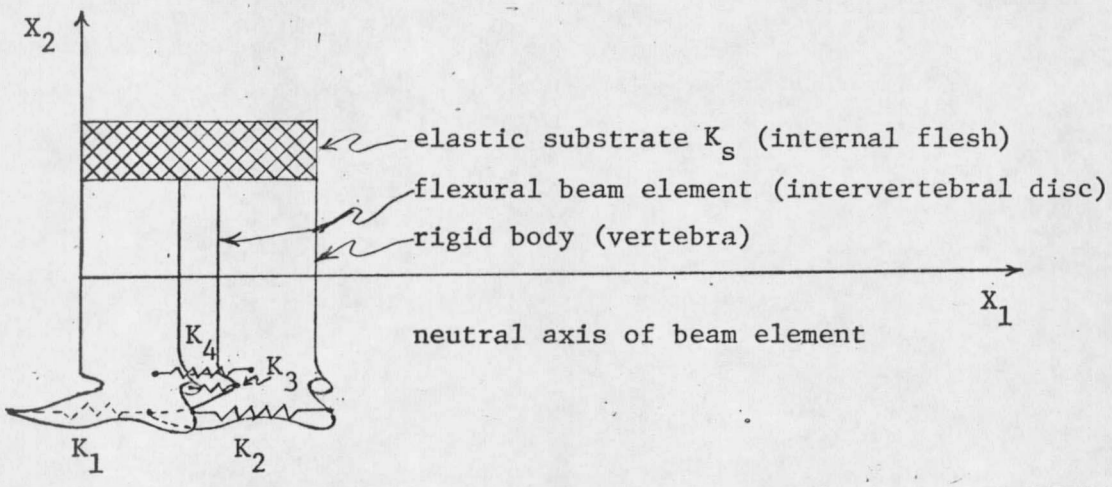


Figure 4-1.--Modeling concepts of vertebral column.

The elastic substrate K_s in Figure 4-1 represents the internal organs and flesh that the vertebral column contacts on its anterior side.

The elongation of each of the springs was dependent on the motion of the intervertebral discs and the geometry of the configuration. The first spring, with stiffness K_1, represents the muscles and ligaments that connect one spinous process of one vertebra to the spinous process of the next vertebra. The second spring, with stiffness K_2, represents the muscles on each side of the spinous process that connect one transverse process of one vertebra to the transverse process of the next vertebra. The third spring, with stiffness K_3, represents the collagen fiber between the inferior and superior articular processes of adjacent vertebrae. The final spring, with stiffness K_4, simulates bone grafted onto the vertebral column for corrective purposes. The muscles that run along the back connecting the vertebrae are treated as if they are segmented muscles connecting one vertebra to another rather than several. Thus, their stiffening effects are incorporated in springs 1, 2, and 3.

The ribs were modeled as curved beam elements with each rib divided into three sections each of constant curvature as shown in Figure 4-2. This was done consistant with the rib geometry defined by Schultz, et. al. [13]. Dimensions of ribs not listed by Schultz were obtained by interpolating between values available. Section OA was assumed to be curved such that it connected perpendicular to the vertebra at O. Point A corresponded to the average data point of Schultz's work. The curvature of DL was set such that its center of curvature was on the X_3 axis as seen in Figure 4-2. A spring, with stiffness K_r, was attached

to the end of the third section (Point 6) of each rib and to a stationary point G, to simulate the sternum rib interaction. All ribs extended at a 25 degree angle anteriorly from the transverse plane of the body.

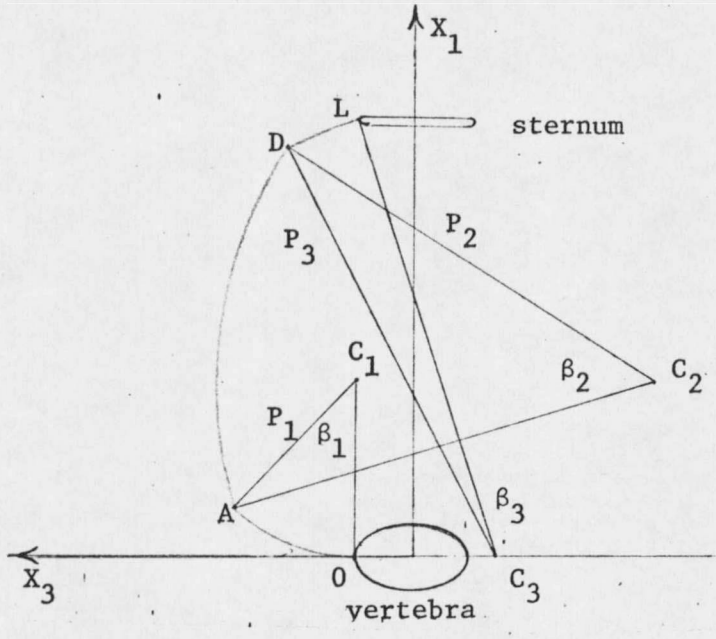


Figure 4-2.--Rib plane configuration

Since the ribs are long slender beams and their curvatures large, the assumption that straight beam theory applied was made. Since the ribs are virtually free to rotate at both the junction with the vertebrae and the sternum, the ribs were assumed to store energy only in bending. The finite element derivation is shown in Appendix I for the curved beam elements.

The head was supported with a spring of stiffness K_h attached to a stationary point G_2. The stiffness K_h, was assumed to be equivalent to

an inch square piece of flesh one eighth of an inch thick. Although the head pivots about the dens of the second cervical vertebra and its motion is controlled by a complex network of muscles, the head was assumed to be rigidly attached to the dens of the second cervical vertebra and the pivot point was the end of the intervertebral disc connecting to the bottom of the second cervical vertebra. The use of a Harrigan rod for the stiffening of the back was modeled as a large spring connecting two vertebrae. These vertebrae are not necessarily adjacent. Other items included in the model were the kinetic energy of the head, the sacral mass, the intervertebral discs, the vertebrae, and the ribs. The schematic of the entire model is shown in Figure 4-3.

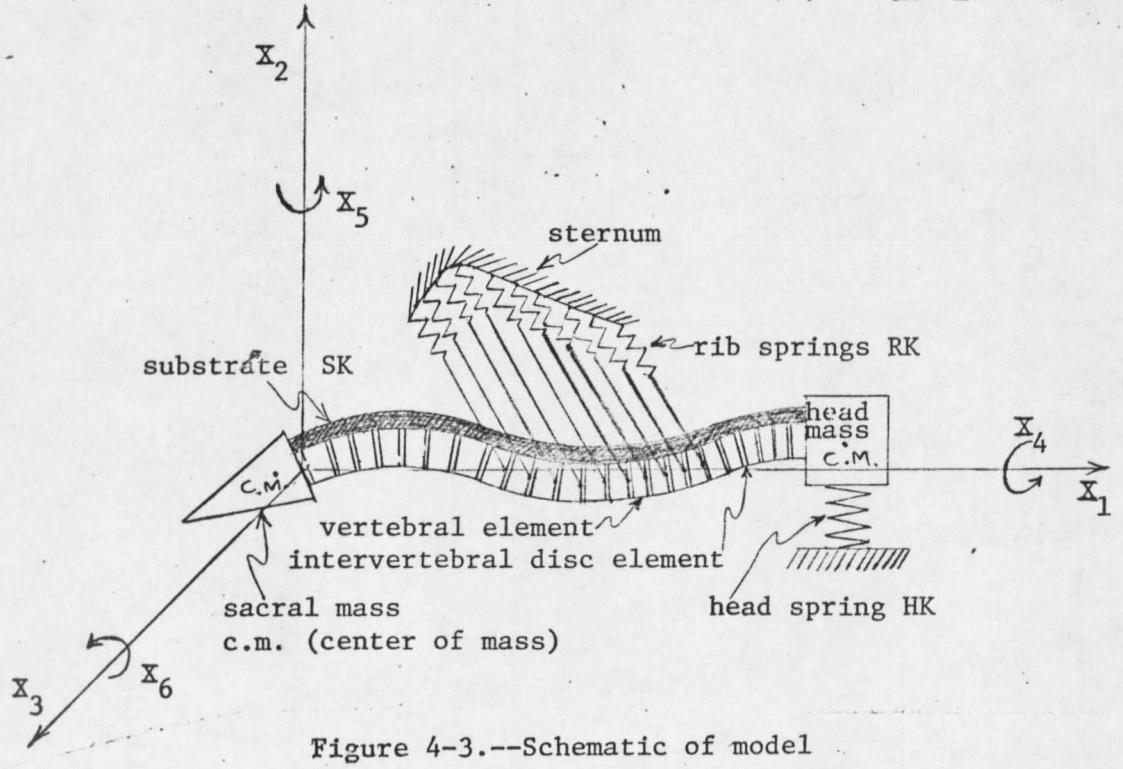


Figure 4-3.--Schematic of model

All elemental stiffness and mass matrices were formulated by the energy method. A formulation of the potential energy of each element can be expressed in tensorial form as follows:

$$V = 1/2\ \underset{\sim}{u}^T\ \underset{\sim}{K}\ \underset{\sim}{u} \tag{4-1}$$

where $\underset{\sim}{u}$ is the displacement vector of that element and $\underset{\sim}{K}$ is the stiffness matrix.

A formulation of the kinetic energy of each element can be expressed in tensorial form as

$$T = 1/2\ \dot{\underset{\sim}{u}}^T\ \underset{\sim}{m}\ \dot{\underset{\sim}{u}} \tag{4-2}$$

where $\dot{\underset{\sim}{u}}$ is the velocity vector of the element and

$\underset{\sim}{m}$ is the mass matrix.

Eulers equation of motion for each finite element is of the form

$$\underset{\sim}{m}\ \ddot{\underset{\sim}{u}} + \underset{\sim}{K}\ \underset{\sim}{u} = \underset{\sim}{Q} \tag{4-3}$$

where $\underset{\sim}{Q}$ is the externally applied force vector. All derivations of elemental stiffness and mass matrices are shown in Appendix I.

Geometric Considerations and Boundary Conditions

It is assumed that the spine, the associated parts, and the applied forces are distributed symmetrically about the sagittal plane of the body. Therefore, the motion of the spine will be symmetric about the

sagittal plane.

Because of the size and stiffness of the sacral mass, it is assumed to be rigid and stationary. The boundary conditions of the spine at the sacral mass are modeled as fixed or pinned.

Other boundary conditions considered were the fixed walls to which the various springs, the head, ribs, and substrate were connected. After applying each of these conditions, the resulting degrees of freedom were: three for each vertebra, six for each intervertebral disc, and twenty-two for each rib, with appropriate interaction and constraints. The first intervertebral disc had only four degrees of freedom for the pinned case and three for the fixed case. The end of the rib connecting to the vertebra was free to rotate on the vertebra but moved with the vertebra. The resulting system had 270 degrees of freedom for the pinned case and 269 degrees of freedom for the cantilevered case.

Input Parameters

All vertebral dimensions were obtained from the skeleton of an adult male whose age at death was over twenty. Those dimensions measured were body height, the cross-sectional dimensions of the body, and distances from the center line of the body to various ligaments and muscle connections. The cross-sectional configuration of the intervertebral disc was assumed to be the same as that of the vertebra body

surface immediately above it.

Thicknesses of the intervertebral discs were obtained from the work of Orne and Liu [5]. The moment of inertia used in the bending energy formulation for each intervertebral disc was assumed to be the same as that of the characteristic cross-section of the vertebral body surface immediately above it. Inertia values of the intervertebral discs were comparable to those obtained by Orne and Liu.

Initial stiffnesses for ligaments and muscles connecting the various processes of the vertebrae were obtained from Schultz et. al. [14]. They found the stiffness of the ligaments connecting the transverse processes of consecutive vertebrae to vary from 112 to 56 #f/in with the stronger ligaments in the lower lumbar and the weaker ligaments in the upper thoracic. The stiffness of the ligaments connecting the spinous processes varied from 56 to 28 #f/in while the stiffness of the muscle combination of the spinalis dorsi and semispinalis dorsi varied from 140 to 84 #f/in. Values for the stiffness of the collagenous material connecting the inferior and superior articular processes and the muscles and ligaments in the cervical region were assumed. The stiffness of the muscles and ligaments along the spine were assumed to vary linearly in the lumbar and thoracic regions. In the cervical region, the stiffnesses associated with the first thoracic vertebra muscles and ligaments were used for each of the cervical vertebrae. The collagenous material connecting the inferior and superior processes was assumed to be the

same stiffness as the ligaments connecting the spinous process.

The value used for the modulus of elasticity for the intervertebral disc was 22,500 psi. This value was changed on several runs to determine its affect on the model.

The values of the skin stiffnesses were formulated as

$$\frac{F}{\delta} = K = EA/L \quad \text{(Force/Length)} \tag{4-4}$$

The value of E for flesh was assumed to be that determined by Goldman and Van Gierke (1960) as stated by Spiegl and Jurist [15] 7.5×10^4 dynes/cm^2 (1.09 #f/in^2). The skin thickness on the head was assumed to be 1/8 of an inch and thus for a cross-section of one square inch, the head flesh stiffness, K_H, was determined to be 8.72 #f/in. This compares to the value of 2.14 #f/in used by Spiegl and Jurist as the skin stiffness for tissue next to the ulnar head and the value of 12.56 #f/in used by Spiegl and Jurist again in the simulation of tissue composed of ligaments, articular cartilage, and surrounding flesh.

Since more flesh is found under the vertebral column that is found in the thin layer around the head, the effective length of flesh that the vertebral column was assumed to deflect was chosen as one half an inch resulting in a stiffness of four times less than the head spring constant. The elastic energy of the substrate was expressed as

$$V_s = 1/2 \int_0^{\ell} K_s \, u_2(X_1)^2 \, dX_1 \tag{4-5}$$

Thus, the value of K_s is per unit length and is 2.18w ($\#f/in^2$) where w is the width of the particular element in question in inches. The sternum rib flesh was assumed to have a cross-sectional area of one inch square and an effective length of one-half inch resulting in an K_r value of 2.18 #f/in.

The resulting stiffness increase due to spinal fusion was treated in the same manner as the rib flesh. The modulus of elasticity used in Equation 4-4 was 2×10^6 psi, the value used by Grammens [16] for bone. The strips of bone grafted onto the vertebrae were .393 inches wide (1 cm) and .197 inches thick (.5 cm). Their effective length was assumed to be the length of the intervertebral disc it covered since it was this portion that was assumed to stretch when the intervertebral disc flexed. Thus, the resulting stiffness associated with each intervertebral disc where a fusion was made was $1.55 \times 10^5/L$ (#f/in) where L was the intervertebral disc length.

The stiffness of the Harrigan rod was also defined by Equation 4-4. The Harrigan rod is constructed of steel with a modulus of elasticity of 30×10^6 psi. The Harrigan rod modeled in this analysis was three eighths of an inch in diameter and seven inches long.

The rib cross-sectional dimensions were measured from a skeleton for each of the three divisions of the rib. They were found to be elliptic in cross-section and treated accordingly in the computation of moment of inertia values. The E value for compact bone was 2.0×10^6

psi as used by Grammens [16].

The volume of each vertebra was determined experimentally. The density of bone used for the vertebrae was .076 #m/in^3, as suggested by Nickell and Marcal [17]. Since the vertebral center of mass does not coincide with the centerline of the vertebral body, the eccentricity distances determined by Orne and Liu [5] were used. For detail of geometry see Figure I-5 in Appendix I.

The density was 0.076 #m/in^3 for bone and 0.058 #m/in^3 for intervertebral disc. The mass of the head was 7.5 #m. The density of average tissue was assumed to be 0.051 #m/in^3, a value between the density of skin and bone. The sacral mass value was 0.246 #m as attained from Krogman [18].

Reduction of Coordinates

The solving of the resulting 270 and 269 degree of freedom systems directly required an immense amount of computer storage and computer time. Therefore, a reduction of coordinate scheme was developed in accordance with the method described by Anderson [19] and Meirovitch [20]. Assumed modes of vibration intended to approximate the motion of the vertebral column and ribs were developed. Referring to Figure 4-3, seven modes dealt with assumed deflections of the spine in the X_2 direction, five modes dealt with assumed deflections of the spine in the X_1 direction, and four modes dealt with possible bending modes of the

ribs. The first X_2 displacement mode had displacements increasing linearly with X_1 with zero deflection at the sacrum connection. The next five modes of assumed deflections in the X_2 direction were sine waves of one through five nodes. The seventh X_2 mode had the cervical spine above the first rib deflected into a half sine node shape. The X_2 displacement modes are shown in Figure 4-4 with the exception of modes five and six.

The first mode in the X_1 direction had displacements which vary linearly with X_1. The next four X_1 assumed modes are sine waves of one through four nodes.

Each of the rib's three sections were assumed to change curvature by a specified amount and the resulting global deflections used as mode shapes.

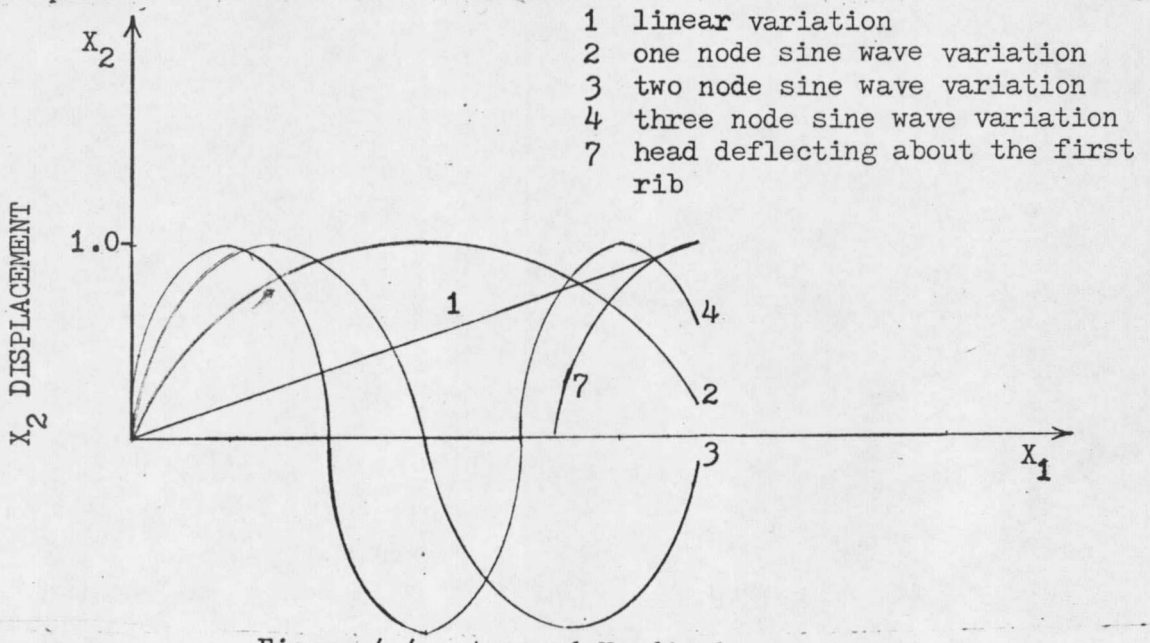


Figure 4-4.--Assumed X_2 displacements.

Changes in curvature were expressed as

$$R_1 \beta_1 = R_1' \beta_1' \qquad (4\text{-}6)$$

where R_1 and β_1 are the radius of curvature and included angle, the prime indicates the value in the deflected position. The rotation of the rib in the plane of the rib about the connection to the vertebra was assumed to be half the difference between β_1 and β_1'. This assumption was also made for the connection of the ribs to the sternum. Although all ribs were assumed to deflect in this fashion, the amount each rib deflected was different. The first rib mode has all ribs deflecting in this fashion. Rib mode two was the same as the first mode except the degree each rib deflected varied sinusoidally from the first to the tenth rib. The third rib mode was similar to mode two except the vertical variation was a cosine wave. The last rib mode is the same as rib mode two with the exception that the variation in displacement is a double node sine wave. The assumed rib modes are considered independent of the vertebral column and cause no resulting vertebral motion. This allows for the possibility of the ribs vibrating on the spine with no vertebral motion. The resulting displacements of the ribs due to the assumed X_1 and X_2 displacement modes of the spine are included in each respective X_1 and X_2 spine mode. This motion was set such that the sternum end of the rib stayed within the plane of the undisplaced rib.

In accordance with the method described by Anderson [19], the pre-

vious assumed modes are combined in the form

$$\{x\} = [\gamma]\{p\} \tag{4-7}$$

where $\{x\}$ = global displacement vector,

$\{p\}$ = reduced coordinate vector, and

$[\gamma]$ = transformation matrix.

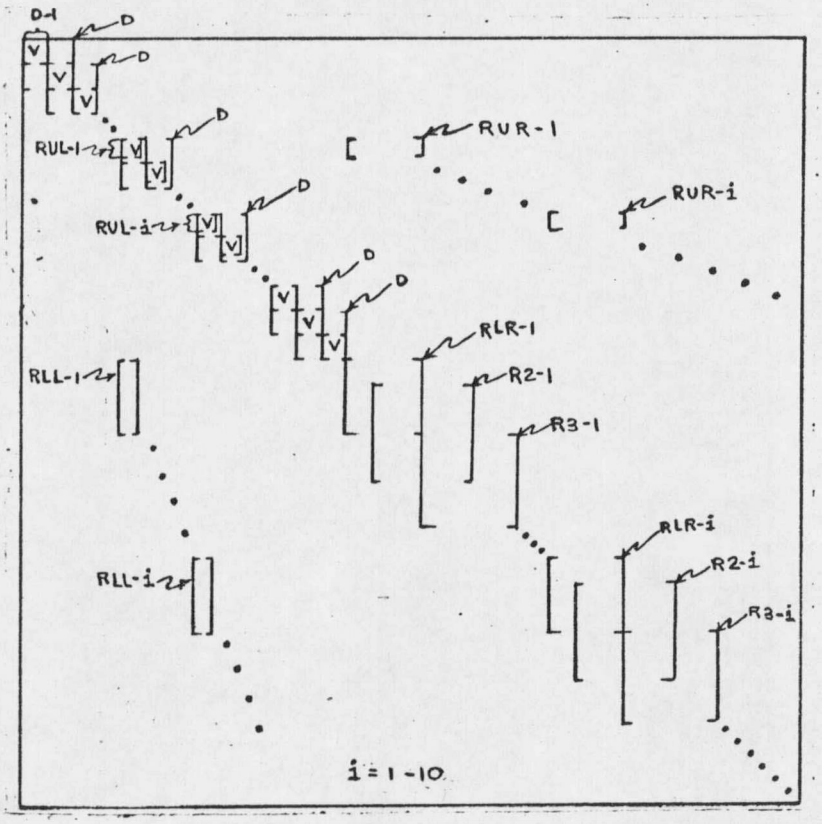
The columns of the transformation matrix are the assumed modes.

To avoid forming the massive global coordinate matrices, each elemental stiffness and mass matrix was expressed in terms of the reduced coordinate system and added appropriately to form a global reduced mass and stiffness matrix. The form of the global stiffness matrix is illustrated in Equation 4-8 for the fixed sacral condition.

An explanation of each symbol in Equation 4-8 is as follows:

In Equation 4-8, each V represents a 3 x 3 vertebral matrix, while each D represents a 6 x 6 intervertebral disc matrix, and each RUL-i represents the upper 2 x 2 matrix of the first rib sections matrix. The RLL-i matrix represents the lower left 9 x 2 matrix of the first rib sections matrix. Each RUR-i represents the upper right 2 x 9 matrix of the first rib sections matrix, and each RLR-i represents the lower right 9 x 9 matrix of the first rib sections matrix. Lastly, the R2-i represents the 12 x 12 matrix of the second rib section, and each R3-i represents the 11 x 11 matrix of the third rib section.

$$[K] = \quad (4\text{-}8)$$



The first intervertebral disc matrix D-1 was a 3 x 3 matrix for the fixed end case and a 4 x 4 matrix for the pinned end case. There was no interaction assumed between ribs, thus, the matrices associated with the ribs did not overlap.

Each of the elemental matrices of the rib sections was a 12 x 12 matrix. However, when transformed into global coordinates, by boundary conditions, motion in the X_3 direction was zero for the end of the first rib section attached to the vertebra and for the end of the third rib section attached to the sternum. This eliminated the degree of freedom

associated with that direction and thus the row and column associated with that direction were removed from the matrix reducing it to a 11 x 11.

The end of the rib which was connected to the vertebra had the same displacements as its associated vertebra but not the same rotations; hence, the first rib section matrix was broken up as shown in the global matrix Equation 4-8. The elemental matrices that remained intact and were not reduced in size, could be transformed directly from the elemental form to the reduced global coordinate form. This procedure applied to the vertebral matrices, intervertebral disc matrices, and second rib section matrices. Shown below is the transformation of the vertebral matrix to the reduced coordinate system.

$$[\overline{Rv}_i] = [\overline{\gamma}_{vi}]^T [Tv_i]^T [V_i] [T_{vi}] [\overline{\gamma}_i] \qquad (4\text{-}9)$$

where $[\overline{Rv}_i]$ = global reduced matrix (N x N) associated with $[V_i]$,

$[\overline{\gamma}_{vi}]$ = portion of $[\gamma]$, (3 x N), associated with $[V_i]$,

$[Tv_i]$ = transformation matrix, (3 x 3), associated with $[V_i]$,

and N = number of reduced coordinates.

The intervertebral disc matrices required a transformation which converted the "end one" global displacements of the intervertebral disc to the "end one" global displacements of the vertebra it attached to. The nomenclature for "end one" and "end two" is illustrated in Figure 4-5.

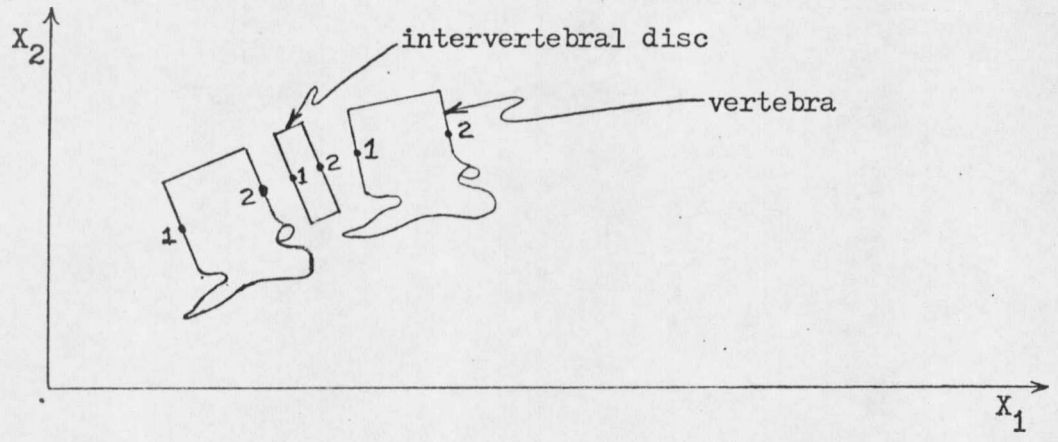


Figure 4-5.--Elemental end nomenclature (end 1 displacements of the intervertebral disc must be expressed in terms of end 1 vertebral displacements.

Thus the reduced intervertebral disc matrices are obtained as follows:

$$[\bar{R}_{Di}] = [\bar{\gamma}_{Di}]^T[T_{2Di}]^T[T_{1Di}]^T[D_i][T_{1Di}][T_{2Di}][\bar{\gamma}_{Di}] \qquad (4\text{-}10)$$

where $[\bar{R}_{Di}]$ = global reduced matrix (N X N) associated with $[D_i]$,

$[\bar{\gamma}_{Di}]$ = portion of $[\gamma]$, (6 x N), associated with $[D_i]$,

$[T_{1Di}]$ = transformation matrix, (6 x 6) associated with $[D_i]$,

and $[T_{2Di}]$ = transformation matrix, (6 x 6), associated with putting end one global displacements of the intervertebral disc in terms of end one global displacements of the vertebra directly associated.

For the third rib section elements, the transformation to global coordinates was made first; then the appropriate row and column associated with end two X_3 displacements eliminated since they were zero.

The first rib section matrices were treated in the same fashion as the intervertebral disc matrices.

Method of Solution

The resulting equation of motion (Equation 4-11) in the reduced coordinate system is

$$[\bar{M}]\{\ddot{\bar{P}}\} + [\bar{K}]\{P\} = \{\bar{Q}\} \qquad (4\text{-}11)$$

where $[\bar{M}] = [\gamma]^T[M][\gamma]$,

$[\bar{K}] = [\gamma]^T[K][\gamma]$, and

$[\bar{Q}] = [\gamma]^T\{Q\}$.

The solution of the homogenous part of Equation 4-11 for mode shapes [u] and natural frequencies ω_i was obtained using the sweeping matrix technique [19].

CHAPTER V

FREQUENCY RESPONSE

After solving the homogeneous equation, the response of the system to harmonic excitation is easily obtained. For the reduced coordinate system, the equation of motion is 4-11. The reduced coordinate system equations are transformed to an uncoupled form of the reduced system which results in the equation of motion

$$[\overline{\overline{M}}]\{\ddot{\eta}\} + [\overline{\overline{K}}]\{\eta\} = \{N\} \tag{5-1}$$

where $[\overline{\overline{M}}] = [u]^T[\overline{M}][u]$,

$[\overline{\overline{K}}] = [u]^T[\overline{K}][u]$, and

$\{N\} = [u]^T\{\overline{Q}\}$.

Equation 5-1 represents a set of N uncoupled differential equations of the form

$$\ddot{n}_r(t) + \omega_r^2\, n_r(t) = N_r(t) \quad r = 1, 2, \ldots N \tag{5-2}$$

where ω_r is the natural frequency,

$\omega_r^2 = \overline{\overline{K}}_r/\overline{\overline{M}}_r$

$N_r(t) = (N_r \sin\omega_d t)/\overline{\overline{M}}_r$, and

ω_d = driving frequency.

The steady-state solution is

$$\eta_r(t) = \left(\frac{(N_r/\overline{\overline{M}}_r)\ \omega_r^2}{1 - \omega_r/\omega_d}\right)\sin\omega_d t \tag{5-3}$$

Thus the amplitude response of the system is proportional to the term in parenthesis of Equation 5-3 or

$$R_r = \frac{(N_r/\overline{M}_r)\omega_r^2}{1 - \omega_r/\omega_d} \tag{5-4}$$

Consequently, from the N response Equation 5-4, a vector {R} of length N can be obtained that represents the response of the system in the reduced natural coordinate system to a driving force at frequency ω_d.

The response in the global coordinate system is then

$$\{X\} = [\gamma][u]\{R\}. \tag{5-5}$$

The frequency response was obtained for three driving frequencies evenly spaced between each natural frequency. The response at each natural frequency was taken to be the sum of the two values plotted on each side of it. To simulate damping, the points after each natural frequency were divided by 2^{r-1}, where r corresponds with that natural frequency preceding those points.

CHAPTER VI

RESULTS

The model parameters were adjusted until an experimental frequency response plot for a 22-year old male's spine was closely duplicated. It was determined that the main stiffness parameters contributing to the analytic frequency response plot were the modulus of elasticity values for the intervertebral discs and ribs. The ligament and muscle stiffness values listed in Chapter IV were doubled resulting in a negligible effect on the natural frequencies and the frequency response plot obtained analytically. The effect on the natural frequencies and the frequency response plot was even less noticeable when the substrate, head spring, and rib spring stiffness values were doubled. Therefore, the variational analysis of the frequency response with change in stiffness parameters was limited to the intervertebral disc and rib modulus of elasticity values. The only mass value varied was the head mass which resulted in a noticeable effect on the analytic natural frequency values attained.

Natural Frequencies and Mode Shapes

Figures 6-1a to 6-1f are the first six mode shapes of the normal spine attained by this analysis. The natural frequencies listed below the figures are for the stiffness parameters listed in Chapter IV. The subscript f refers to the fixed vertebral column and subscript ρ refers to the pinned vertebral column.

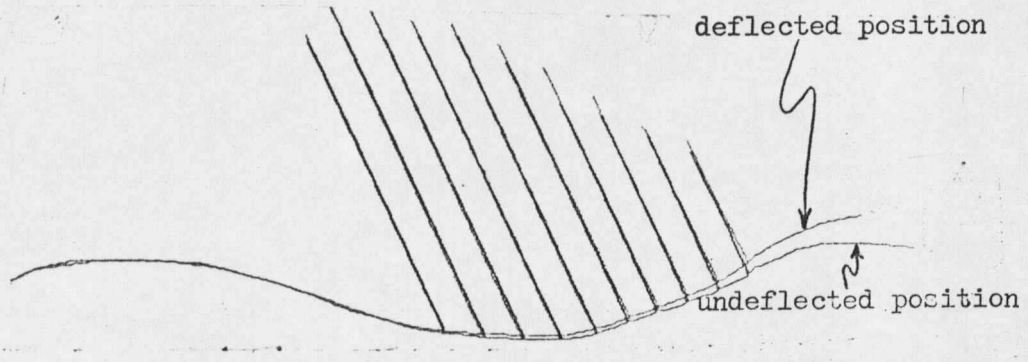


Figure 6-1a.--First bending mode of the spine

F_f = 9.22 Hertz, and

F_ρ = 9.21 Hertz.

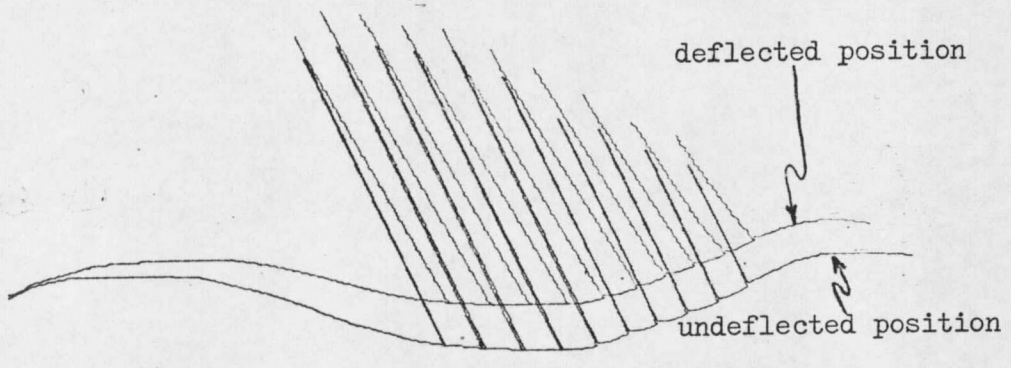


Figure 6-1b.--Second bending mode of the spine

F_f = 69.74 Hertz, and

F_ρ = 66.19 Hertz

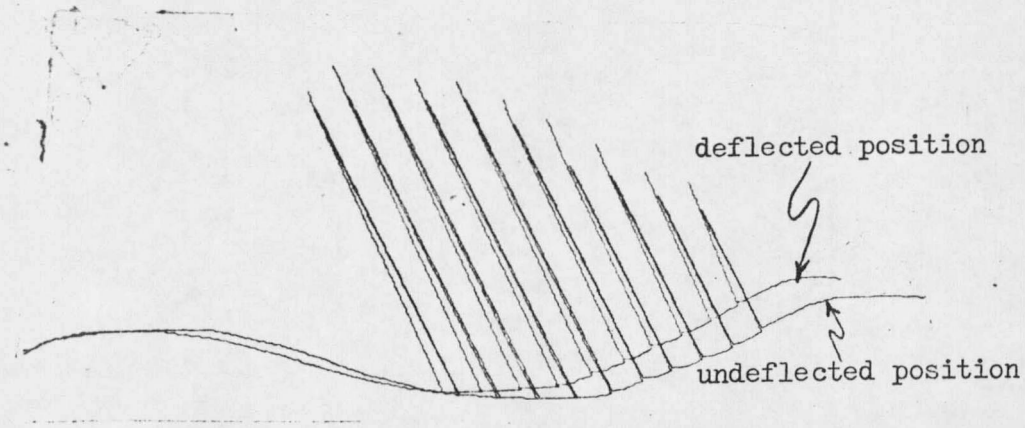


Figure 6-1c.--Third bending mode of the spine

F_f = 81.27 Hertz, and

F_ρ = 81.43 Hertz.

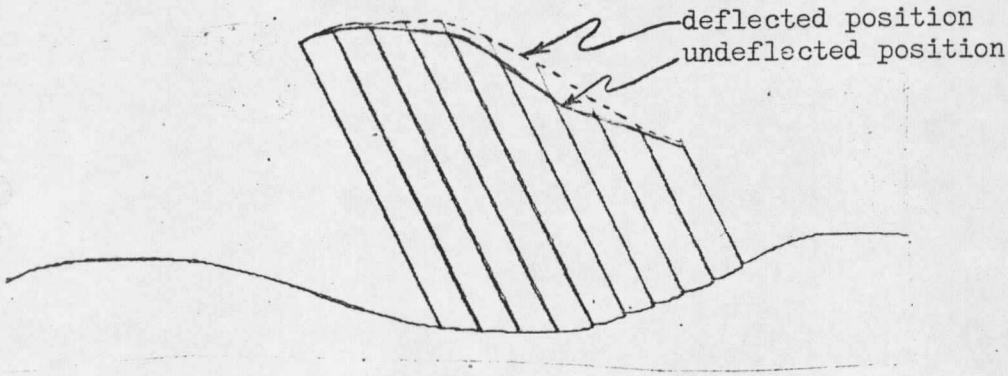


Figure 6-1d.--First bending mode of the ribs

F_f = 119.8 Hertz, and

F_ρ = 119.8 Hertz.

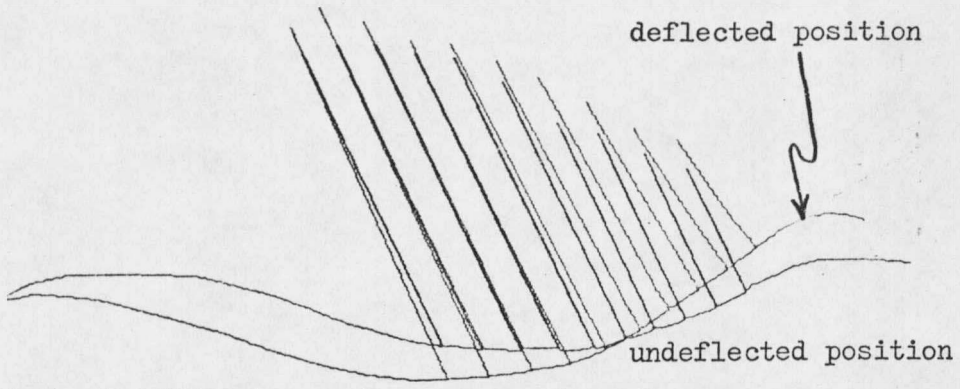


Figure 6-1e.--Fourth bending mode of the spine

F_f = 195.2 Hertz, and

F_ρ = 183.3 Hertz.

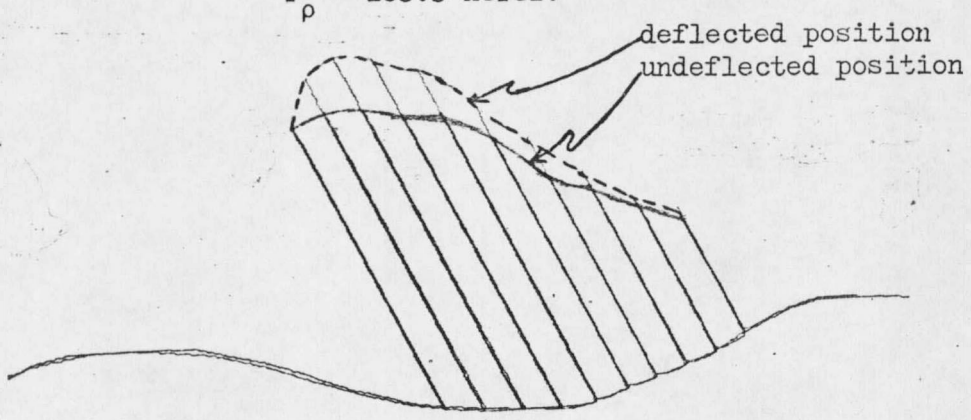


Figure 6-1f.--Second bending mode of the ribs

F_f = 198.2 Hertz, and

F_ρ = 197.4 Hertz.

Figure 6-1a is characteristic of head motion deflecting the vertebral column. Figures 6-1b, 6-1c, and 6-1e depict the motion associated

with the higher bending modes of the spine. Figures 6-1d and 6-1f are the first and second bending modes of the ribs vibrating independent of the vertebral column. The rib mode motion is hard to visualize since the ribs stay in the same plane when deflected thus the dotted lines were drawn to show the rib motion. The last ten mode shapes and natural frequencies obtained analytically are not listed. They do not contribute to the frequency response of the spine for the 30 to 500 hertz range obtained experimentally.

Parameter Variation Analysis

As was stated earlier, only changes in the rib and intervertebral disc modulus of elasticity parameters resulted in a significant change in the natural frequencies. Thus the parametric variation analysis was done by fixing one of these two parameters at the value listed in Chapter IV and varying the other by $\pm$ 20 percent in steps of 10 percent. All other stiffness values were fixed at the values listed in Chapter IV. In Figure 6-2 is the graph for the change of the first natural frequency of the spine for both variations studied. The notation $\overline{E}_R$ refers to the case where the rib bone modulus was held constant while the notation $\overline{E}_D$ refers to the case where the intervertebral disc modulus was held constant. The change in this first natural frequency for the pinned vertebral column case is virtually the same.

Figure 6-3 shows this same analysis as applied to the second and

third frequencies of the spine.

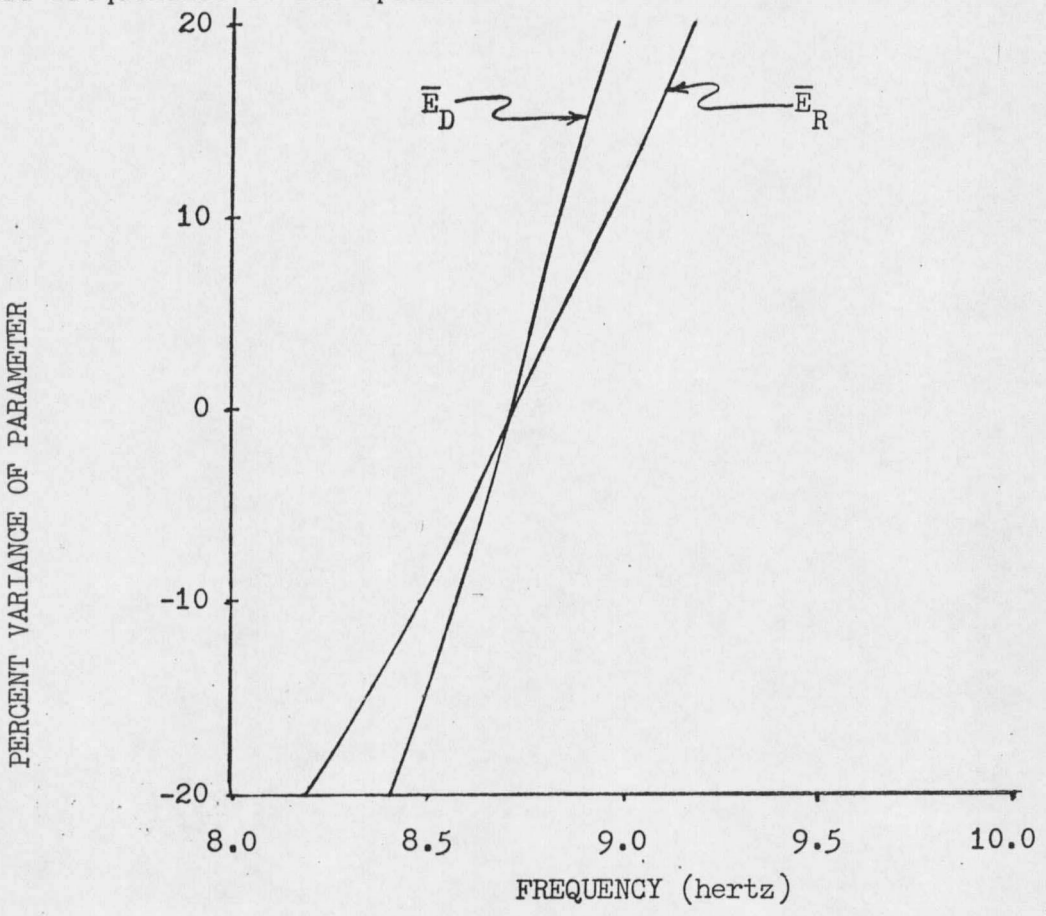


Figure 6-2.--Change in first natural frequency of the spine with respect to stiffness parameters; fixed vertebral column.

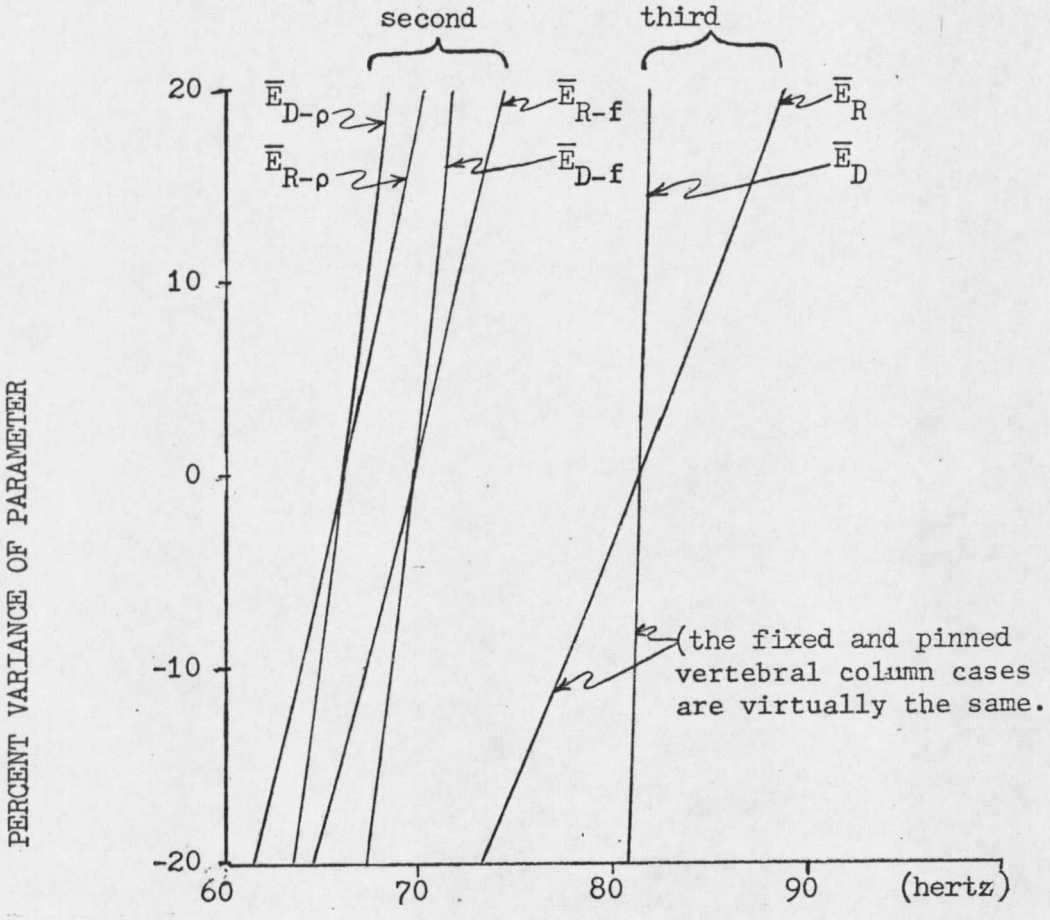


Figure 6-3.--Change in second and third natural frequencies of the spine with respect to stiffness parameters. Subscript -ρ refers to pinned vertebral column, subscript -f refers to fixed vertebral column case.

Figure 6-4 shows this same analysis applied to the fourth bending mode of the spine. For both cases, pinned and fixed, the variance of

the rib modulus of elasticity results in a small change in the higher vertebral natural frequencies compared to the variance of the intervertebral disc modulus of elasticity. Nevertheless, the effect of the rib modulus of elasticity on the first and second vertebral frequencies is significant implying that the ribs cannot be ignored in a spinal frequency analysis.

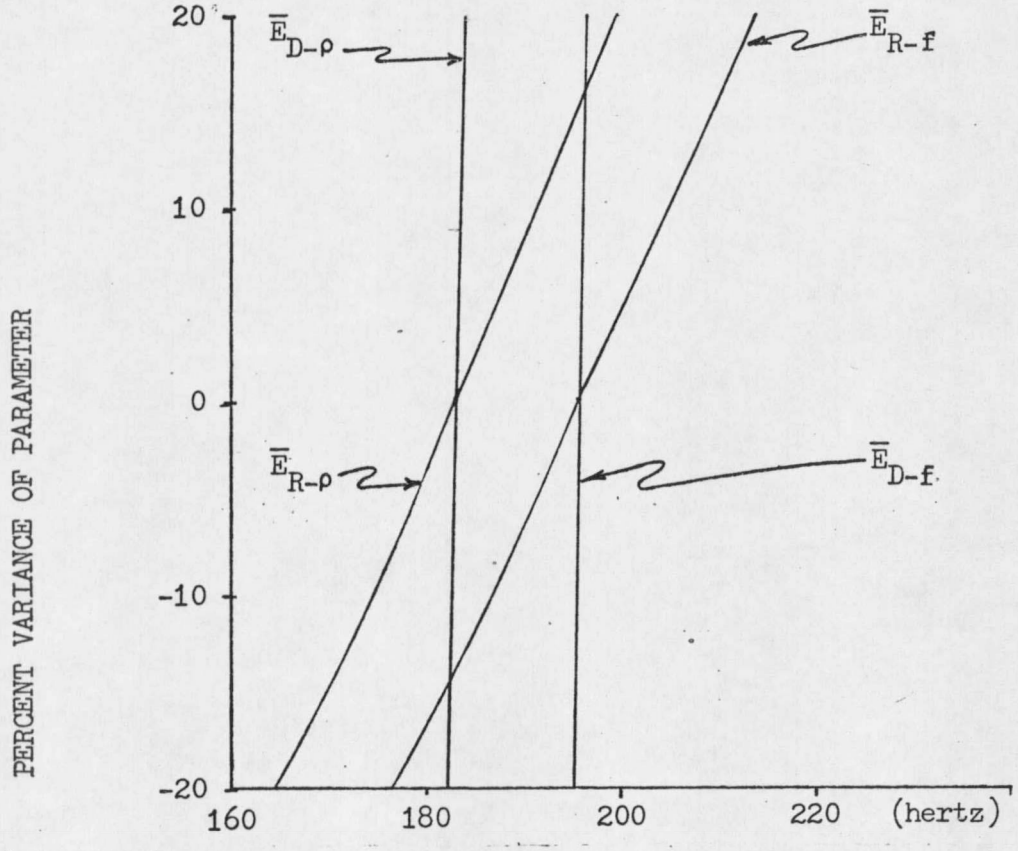


Figure 6-4.--Change in fourth natural frequency of the spine with respect to stiffness parameters. Fixed and pinned vertebral column cases are designated by subscripts -f and -ρ respectively.

Figure 6-5 illustrates the variation of the analysis as it applies to the first two bending modes of the ribs. The pinned vertebral column case is not graphed for clarity but is virtually identical to Figure 6-5. For the rib frequencies, the change in the modulus of elasticity of the intervertebral discs has even less effect on the rib natural frequencies than the change in rib modulus of elasticity had on the vertebral natural frequencies.

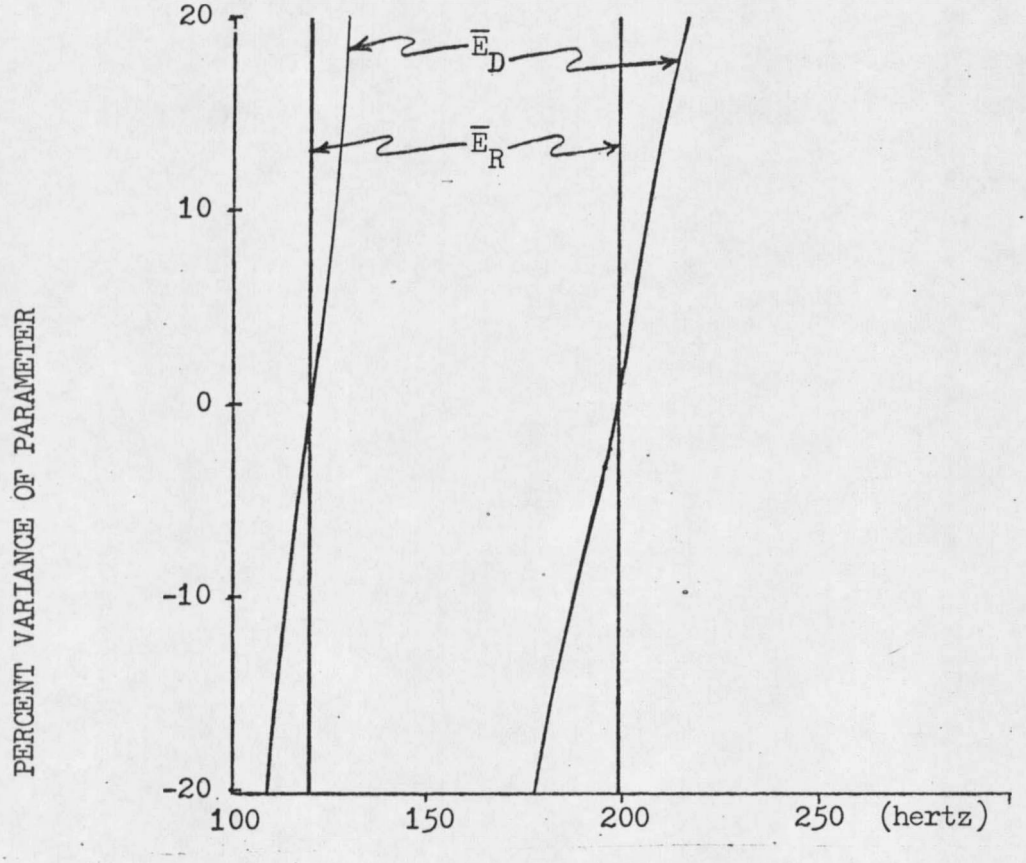


Figure 6-5.--Change in the first and second natural frequencies of the ribs with respect to stiffness parameters; fixed vertebral column case only.

Using the stiffness parameters listed in Chapter IV and varying the head mass resulted in significant changes in the vertebral frequencies and no change in the rib frequencies. The variation of the first vertebral frequency due to head mass variance is shown in Figure 6-6.

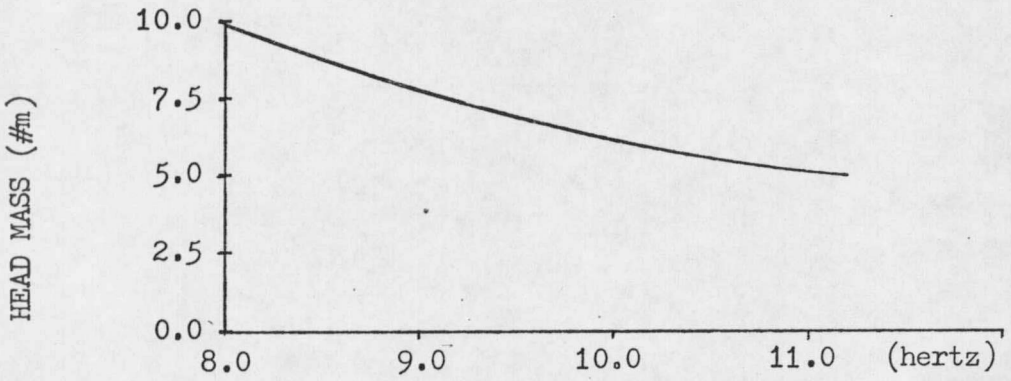


Figure 6-6.--Change in first vertebral frequency due to head mass variance.

Figure 6-7 shows the change in the second and third vertebral frequencies due to head mass variance. The fourth vertebral frequency does not change with head mass variance.

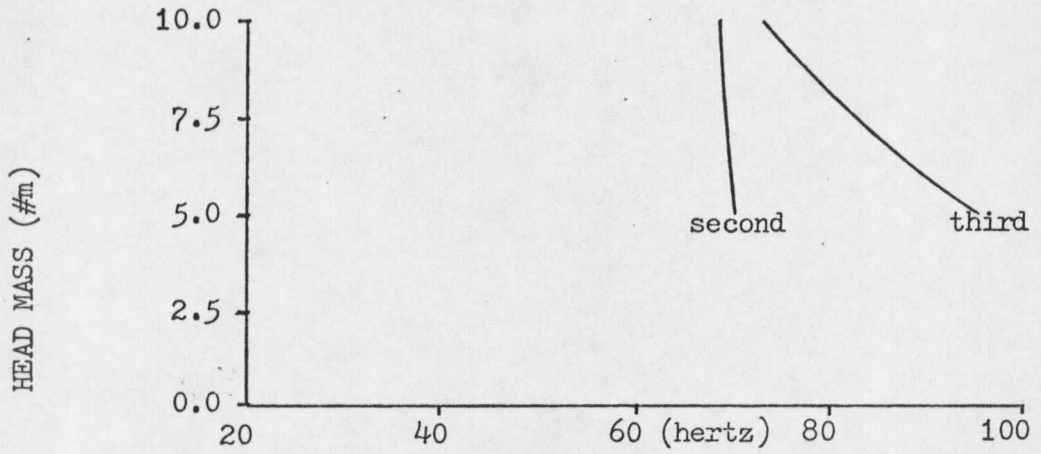


Figure 6-7.--Change in vertebral frequencies two and three due to head mass variance.

Frequency Response

The experimental frequency response plot for the normal spine of a 22-year old male for the frequency range of 30-500 Hertz is shown in Figure 6-8. The analytic frequency response plot for the spine model using the parameters listed in Chapter IV is shown in Figure 6-9.

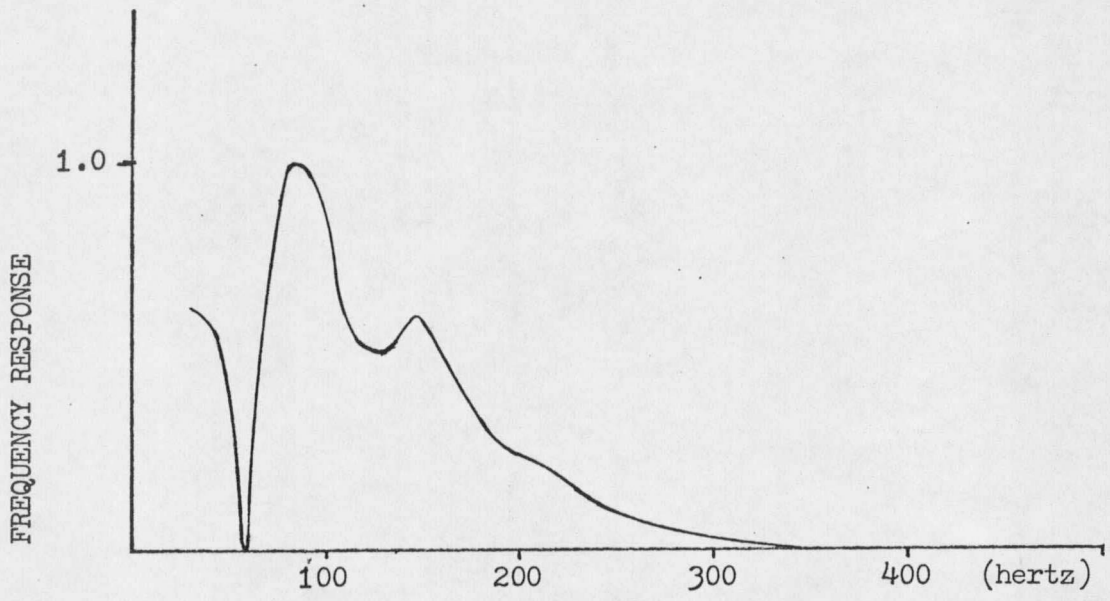


Figure 6-8.--Experimental frequency response of 22-year old male.

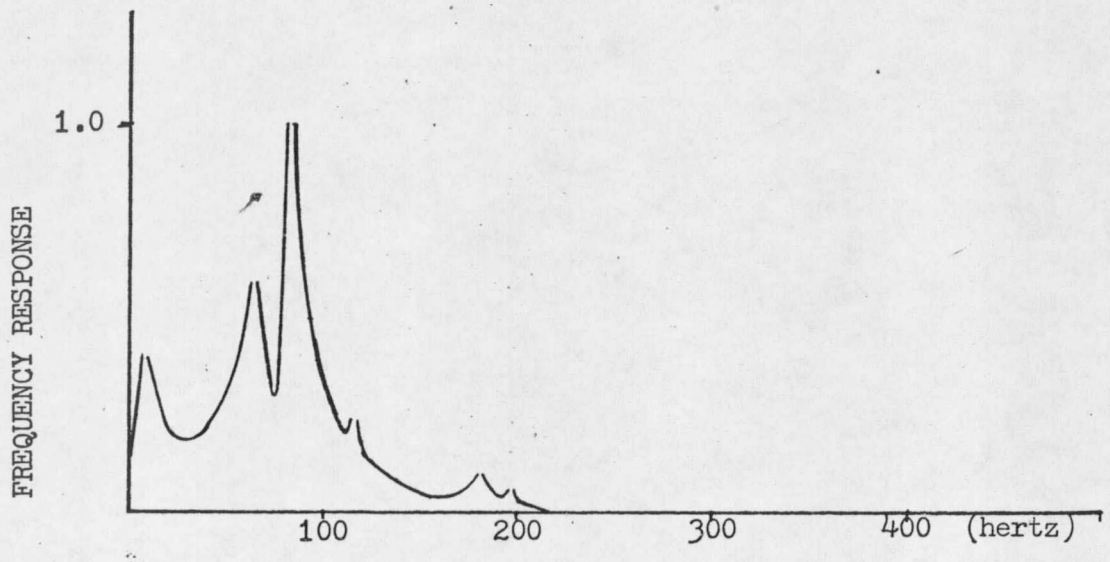


Figure 6-9.--Analytical frequency response (ρ) case.

Both frequency response plots are for a harmonic excitation input at the first lumbar vertebra and the response taken from the first thoracic vertebra. The analytic response is virtually the same for the pinned and fixed vertebral column end conditions except that the pinned condition has peak amplitudes at slightly lower frequencies than the fixed condition. Increasing the intervertebral modulus of elasticity merely shifts the response plot to the right and widens it with higher natural frequencies shifting more than lower natural frequencies. Increasing the rib modulus of elasticity has virtually no effect on the general shape of the curve; however, it moves the natural frequencies at 119 Hertz and 197 Hertz to the right since they are rib modes. Because these rib modes do not cause the spine to move, they do not show up on the experimental response.

Spinal Fusion Results

An analytical solution was attained that simulated the fusion of the fifth thoracic through the first lumbar vertebra both with and without a Harrigan rod. The changes in vertebral natural frequencies are shown in Table 6-1 for the case where all other parameters are fixed at the values listed in Chapter IV.

VERTEBRAL FREQUENCY	CASE 1 (hertz)	CASE 2 (hertz)	CASE 3 (hertz)	PERCENT INCREASE OF 2 OVER 1	PERCENT INCREASE OF 3 OVER 1
1	9.21	9.23	12.4	0.2	34.6
2	66.2	69.8	*	5.4	*
3	81.4	89.2	100.6	9.6	23.6
4	183.3	194.8	287.2	6.3	56.7

Table 6-1.--Changes in analytic vertebral natural frequencies due to spinal fusion.

In Table 6-1, case 1 is the normal spine, case 2 is the normal spine fused from the fifth thoracic to the first lumbar vertebra without a Harrigan rod, and case 3 is case 2 with a Harrigan rod added. All three cases listed are for the pinned sacral case. The * denotes that the second vertebral mode is not excited with the Harrigan rod addition thus the third natural frequency listed is actually the second natural frequency for that case.

From the results listed in Table 6-1, it appears that the changes in vertebral natural frequencies due to fusion are small compared to the changes resulting from the Harrigan rod added in addition to the fusion. The rib natural frequencies are unchanged by the spinal fusion and Harrigan rod.

The motion of the vertebral column associated with each natural frequency is basically the same for the three cases listed in Table 6-1 with the exceptions that points of zero displacement change and the relative motion encountered with each natural frequency change in magnitude. These exceptions are shown in Figures 6-10a through 6-10c.

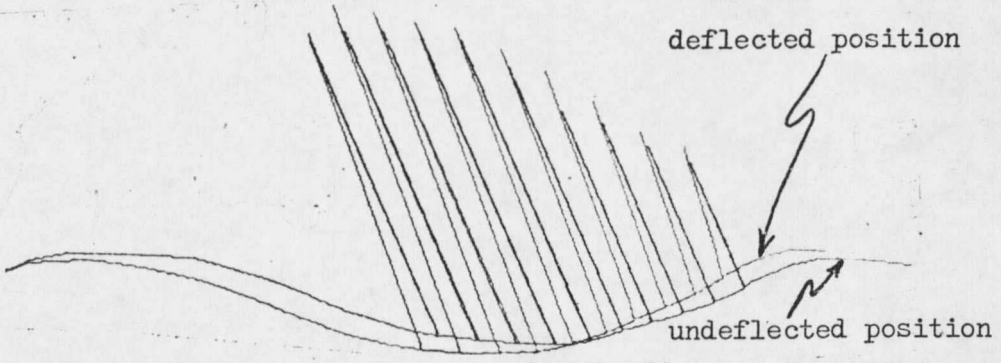


Figure 6-10a.--Motion associated with third natural frequency of normal spine (case 1, Table 6-1).

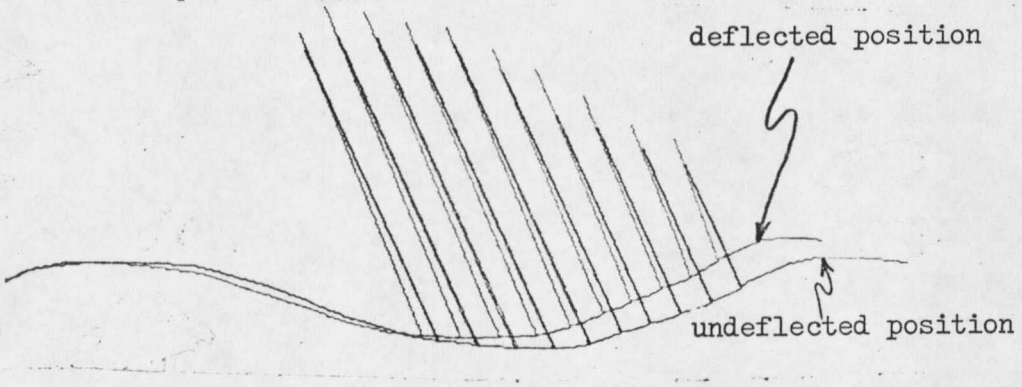


Figure 6-10b.--Motion associated with third natural frequency of fused spine (case 2, Table 6-1).

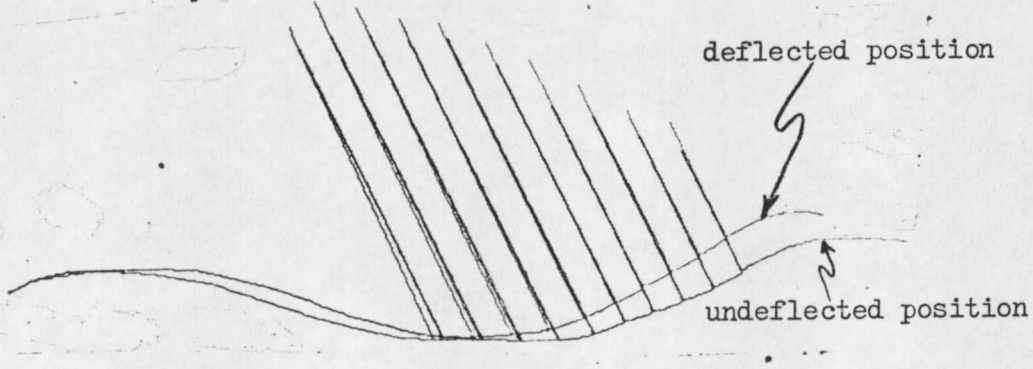


Figure 6-10c.--Motion associated with second natural frequency of fused spine with added Harrigan rod (case 3, Table 6-1, listed

as third natural frequency since it corresponds with the third natural frequency for case 1 and case 2).

The point of zero vertebral displacement occurs below the rib cage for the normal spine in Figure 6-10a, but occurs in the vicinity of the sixth rib connection to the vertebral column for the fused spine case of Figure 6-10b. For the spinal fusion with Harrigan rod implant, the zero vertebral displacement position is slightly below the ninth rib connection to the vertebral column.

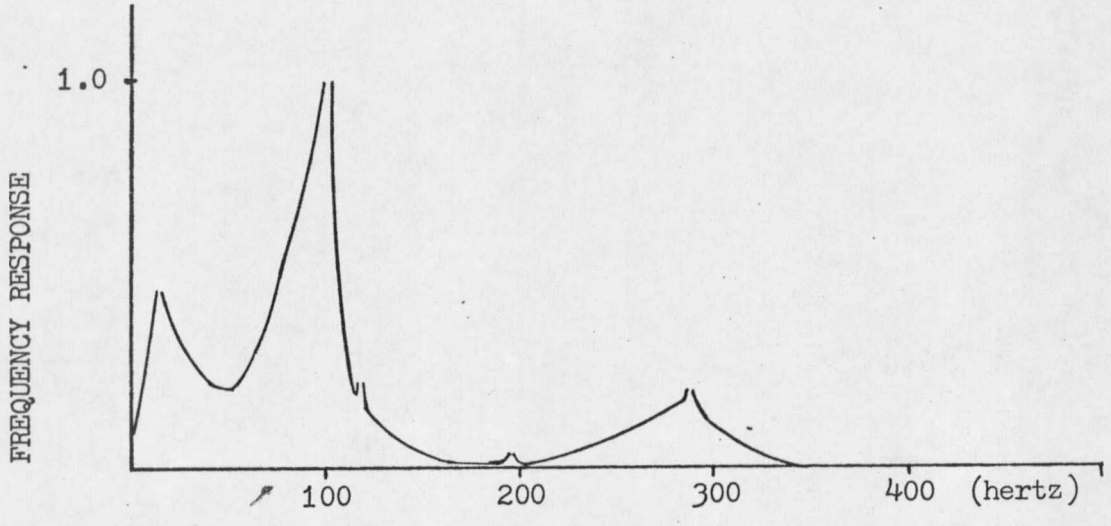


Figure 6-11.--Analytical frequency response plot for the fused spine with Harrigan rod implant.

The analytical frequency response obtained for a spinal fusion is the same as that obtained for a normal spine except for a slight shift to the right of the plot in Figure 6-9. For the spinal fusion with

implanted Harrigan rod, the analytic frequency response plot is shown in Figure 6-11. For this case, there is a large shift to the right for the plot and only one peak in the frequency range from 50 to 110 hertz.

The experimental frequency response for an adolescent female with scoliosis is shown below.

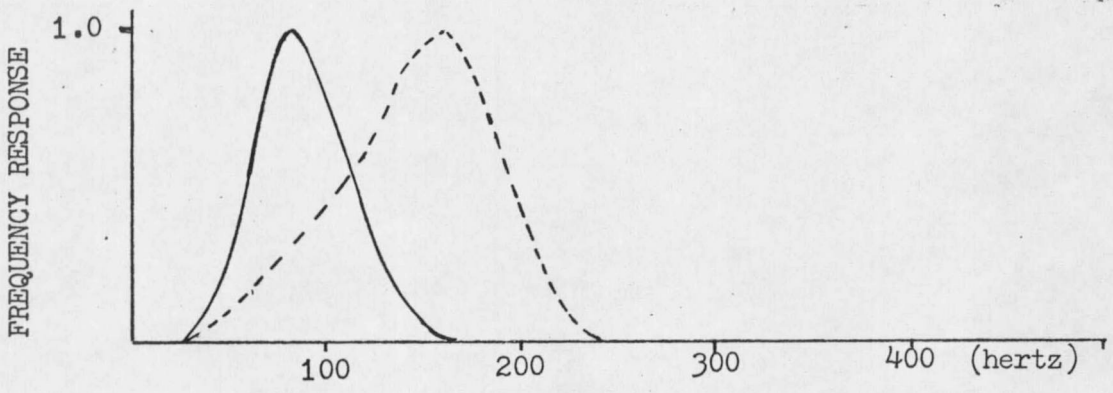


Figure 6-12.--Experimental frequency response plot for scoliotic spine

The solid line plotted in Figure 6-12 is the frequency response plot for the unfused scoliotic spine and the natural frequency is in the same range as that of a normal spine. The dotted line in Figure 6-12 is the frequency response plot for the fused spine with a Harrigan rod implanted. The fusion and Harrigan rod implant was from the fifth thoracic to the first lumbar vertebra as is the case modeled analytically. The correlation between the analytical frequency response and the experimental frequency response is poor. The experimental natural frequency increases two fold from 81 to 164 Hertz while the analytical natural

frequency increases by 23.6 percent from 81 to 101 Hertz. Attention should be directed to the method used to attain this particular experimental frequency response plot. The harmonic excitation device was placed below the lowest fusion sight on the back and the output transducer was placed above the highest fusion sight on the back at the fourth thoracic vertebra. This may be the reason why a second peak or natural frequency does not show on the experimental frequency response plot. According to Figure 6-10b, the zero displacement point of the vertebral motion for the third natural frequency occurs around the fifth thoracic vertebra and thus the higher bending mode may not show. The large difference in analytic and experimental results may be due to the fact that the modeling of the Harrigan rod as a spring does not necessarily take into account the resistance to bending of the spine that the Harrigan rod induces. In addition, the mass, stiffness, and geometric values of the vertebrae, intervertebral discs, ribs and other parts of an adolescents spine may be significantly different from those values used in this analysis. These factors may also contribute to the large difference in the analytic and experimental results for the Harrigan rod fusion case.

CHAPTER VII

DISCUSSION

A model of the human spine has been developed by the finite element technique. The results indicate several bending modes of the spine which may contribute to the response obtained experimentally.

Validity of the Model

The response plots obtained experimentally and analytically are significantly different yet this may be explainable. According to the mode shapes obtained, the first, second, third, and fourth vertebral modes are the main modes contributing to the spinal motion in the thoracic region for the experimental frequency response recorded. The lower modes found analytically are dominant in the experimental response indicating damping in the spinal system. Thus, it is possible that because of damping the transition from the second to the third vertebral mode is not noticeable. Also damping reduces the frequency at which resonance occurs as well as the resonate amplitude. This may well be the case of the fourth vertebral mode, hence reducing the analytical natural frequency from 183 Hertz to the 145 Hertz experimental value. This, however, can only be speculated as the main cause of difference and needs verification. Experimental results need to be obtained that identify the resonating amplitudes of other point along the spine. This allows one to compare experimentally obtained mode shapes with analytically predicted mode shape.

The value of the rib modulus of elasticity 2×10^6 psi correlates well with literature values. The intervertebral disc modulus value is 3.4 times that of Orne and Liu [5]. This discrepancy is not surprising since their value was an estimate obtained from spinal deflection data of Evans and Lissner [21] for the lumbar region. Since this value has seldom been evaluated, it is not surprising to see such a variation. Thus, the parameters used can be cited as pseudoproperties for this particular model and appear to be within the realm of reason.

Comparison to Previous Work

The only previous work found on low amplitude frequency response is that of Adelsbach [12] who developed a finite element viscoelastic model of the vertebral column. His model did not take into account the ribs, head mass, ligaments, or fleshy substrate of the vertebral column. Adelsbach states that the fundamental resonance of the spine was found experimentally to be around 55 Hertz and at 81 Hertz the response was small relative to the 55 Hertz response. This is opposite the finding of this study both analytically and experimentally. In this study, 55 Hertz appears to be close to a minimum response value and 81 Hertz is a natural frequency. Adelsbach also makes no indication of the higher natural frequency found around 145 Hertz on the experimental response plot. The discrepancies are large but may be due to differences in experimental procedures and equipment used to attain the frequency res-

ponse plot.

The Model as a Diagnostic Tool

The model has shown that the fusion of several vertebrae does increase the natural frequencies of the vertebral column. For the case where only a spinal fusion is performed without the added Harrigan rod, the natural frequency change of the third analytical vertebral natural frequency is only eight Hertz. The experimental frequency which has been correlated with this third analytic vertebral natural frequency varies from 70 to 90 Hertz. As a result of this experimental variance, a change of eight Hertz will be virtually impossible to detect unless a more definitive experimental technique is developed. Despite this problem, the indication that the position of zero vertebral displacement changes significantly when a spinal fusion is made may be used as a diagnostic tool to determine if a fusion is successful.

For a spinal fusion with the addition of a Harrigan rod, the correlation between the experimental and analytic natural frequencies is poor and thus, use of predicted natural frequency changes by this model may be impossible for use as a diagnostic tool to monitor healing rates of a fused scoliotic spine. However, the physical details of the implanted Harrigan rod were not available and the modeling of it as a spring between the two vertebrae it connected may not be justified. The use of the position of zero vertebral displacement change may be sufficient to

follow the healing rate progress of the spine for this case but doubtfully. A better understanding of the effects of the Harrigan rod appears necessary before the model can be used for analyzing a spinal fusion with this implant.

APPENDIX I

DEVELOPMENT OF FINITE ELEMENT MATRICES

The coordinate system used for the model is defined below in Figure I-1.

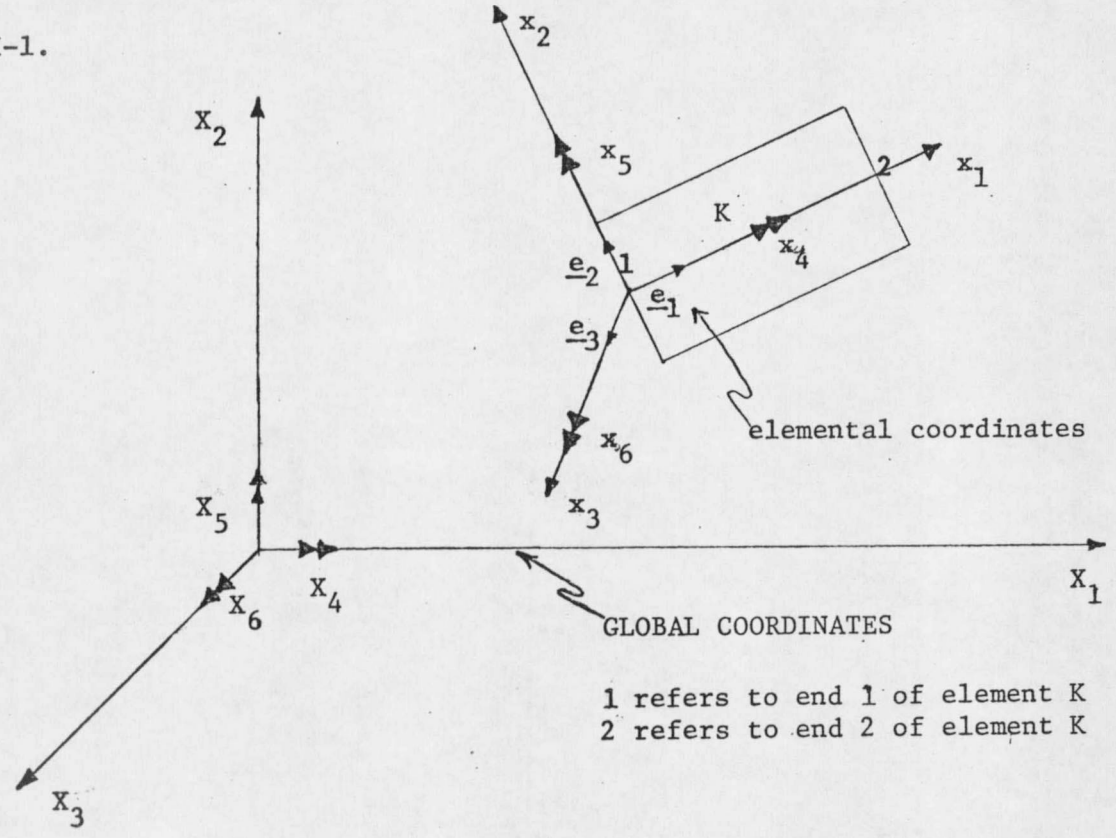


Figure I-1.--Global and elemental coordinate systems

For the elemental coordinate system, the displacements are noted as u_i^j where i refers to the direction or rotation and j refers to the end of the elements in question. For the global coordinate system, the displacements are noted as U_i^j with the same use of i and j. k refers to the kth element.

Formulation of the Spring Stiffness Matrices

All ligaments, muscles, and fusion materials are spring elements whose elongation is determined by the flex of the intervertebral disc. The geometry of this situation is shown in Figure I-2. The linearized elongation of the spring is

$$E_k = (u^2_{1k} - u^1_{1k} + L_k(u^2_{6k} - u^1_{6k}))\underline{e}_1 + (u^2_{2k} - u^1_{2k})\underline{e}_2 \qquad \text{(I-1)}$$

Energy in springs is stored in only the $\underline{e}_1$ direction, thus, the energy stored in each spring V is

$$V = \frac{1}{2} K_k[(u^2_{1k} - u^1_{1k} + L_k(u^2_{6k} - u^1_{6k}))]^2 \qquad \text{(I-2)}$$

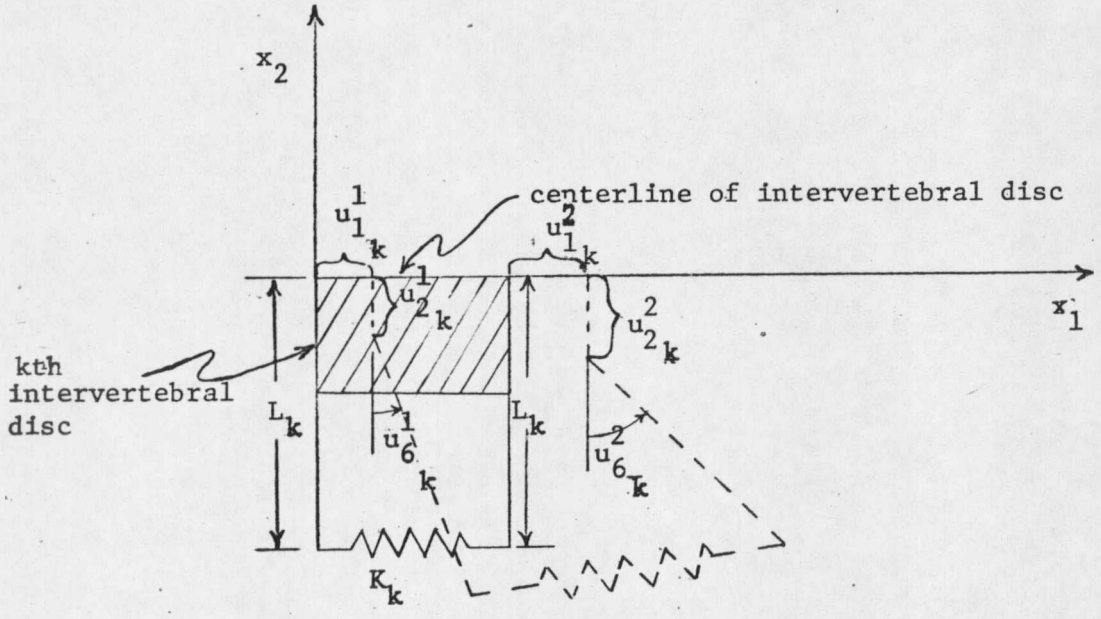


Figure I-2.--Elongation of spring elements

Performing $\partial V/\partial \underset{\sim}{u}$ to Equation I-2 yields I-3 in quadratic form.

$$\underset{\sim}{K}_k \underset{\sim}{u}_k = K_k \begin{bmatrix} 1 & 0 & L_k & -1 & 0 & -L_k \\ 0 & 0 & 0 & 0 & 0 & 0 \\ L_k & 0 & L_k^2 & -L_k & 0 & -L_k^2 \\ -1 & 0 & -L_k & 1 & 0 & L_k \\ 0 & 0 & 0 & 0 & 0 & 0 \\ -L_k & 0 & -L_k^2 & L_k & 0 & L_k^2 \end{bmatrix} \begin{bmatrix} u_1^1 \\ u_2^1 \\ u_6^1 \\ u_1^2 \\ u_2^2 \\ u_6^2 \end{bmatrix} \qquad \text{(I-3)}$$

I-3 is applied to each of the four spring elements each intervertegral disc has. The K_k and L_k values change for each spring. The six by six matrix is the resulting stiffness matrix.

Formulation of the Beam Element Matrix for Intervertebral Discs

The energy stored in bending of a differential element of a beam is

$$dV = \frac{1}{2} EI[u_2'' \quad (X_1)]^2 dX_1 \qquad \text{(I-4)}$$

where u_2 is assumed to be a function of X_1. That assumed function is

$$u_2(X_1) = a_o + a_1 X_1 + a_2 X_1^2 + a_4 X_1^3 \qquad \text{(I-5)}$$

Thus,
$$u_2''(X_1) = 2a_2 + 6a_3 X_1 \qquad \text{(I-6)}$$

and
$$V = \frac{1}{2} EI \int_o^L (2a_2 + 6a_3 X_1)^2 dX_1 \qquad \text{(I-7)}$$

Equation I-7 is for a beam of constant EI. I-7 when evaluated and put in quadratic form is

$$V = \frac{1}{2} EI[a_2 a_3] \begin{bmatrix} 4 & 6L \\ 6L & 12L^2 \end{bmatrix} \begin{bmatrix} a_2 \\ a_3 \end{bmatrix} \tag{I-8}$$

Putting a_2 and a_3 in terms of u_2^1, u_2^2, u_6^1, and u_6^2 yields

$$\begin{bmatrix} a_2 \\ a_3 \end{bmatrix} = \begin{bmatrix} -3L^{-2} & -2L^{-1} & 3L^{-2} & -L^{-1} \\ -2L^{-3} & L^{-2} & -2L^{-3} & L^{-2} \end{bmatrix} \begin{bmatrix} u_2^1 \\ u_6^1 \\ u_2^2 \\ u_6^2 \end{bmatrix} \tag{I-9}$$

Transforming I-8 in terms of u_i^j displacements and performing $\partial V/\partial y$ yields

$$K_{ik} u_k = EI \begin{bmatrix} 0 & 0 & 0 & 0 & 0 & 0 \\ 0 & 12L^{-3} & 6L^{-2} & 0 & -12L^{-3} & 6L^{-2} \\ 0 & 6L^{-2} & 4L^{-1} & 0 & -6L^{-2} & 2L^{-1} \\ 0 & 0 & 0 & 0 & 0 & 0 \\ 0 & -12L^{-3} & -6L^{-2} & 0 & 12L^{-3} & -6L^{-2} \\ 0 & 6L^{-2} & 2L^{-1} & 0 & -6L^{-2} & 4L^{-1} \end{bmatrix} \begin{bmatrix} u_1^1 \\ u_1^1 \\ u_2^1 \\ u_6^1 \\ u_1^2 \\ u_2^2 \\ u_6^2 \end{bmatrix} \tag{I-10}$$

Adding axial stiffness to the beam elements merely adds to the stiffness in the X_1 direction resulting in the following beam stiffness matrix which compares with the results found in Przemieniecki [22] and Zienkiewicz [23].

$$EI \begin{bmatrix} A/IL & 0 & 0 & -A/IL & 0 & 0 \\ 0 & 12L^{-3} & 6L^{-2} & 0 & -12L^{-3} & 6L^{-2} \\ 0 & 6L^{-2} & 4L^{-1} & 0 & -6L^{-2} & 2L^{-1} \\ -A/IL & 0 & 0 & A/IL & 0 & 0 \\ 0 & -12L^{-3} & -6L^{-2} & 0 & 12L^{-3} & -6L^{-2} \\ 0 & 6L^{-2} & 2L^{-1} & 0 & -6L^{-2} & 4L^{-1} \end{bmatrix} \tag{I-11}$$

Formulation of the Substrate Stiffness Matrices

The energy stored in a differential element of the substrate below an intervertebral disc is

$$dV_{s_d} = \frac{1}{2} SK \, (u_2(X_1))^2 dX_1 \tag{I-12}$$

where SK is the stiffness of the flesh substrate. Thus,

$$V_{s_d} = \frac{1}{2} SK \int_o^L (u_2(X_1))^2 dX_1 \tag{I-13}$$

using the same assumed displacement function for u_2 that was used for the beam element results in

$$V_{s_d} = \tfrac{1}{2} SK \begin{bmatrix} a_o & a_1 & a_2 & a_3 \end{bmatrix} \begin{bmatrix} L & L^2/2 & L^3/3 & L^4/4 \\ L^2/2 & L^3/3 & L^4/4 & L^5/5 \\ L^3/3 & L^4/4 & L^5/5 & L^6/6 \\ L^4/4 & L^5/5 & L^6/6 & L^7/7 \end{bmatrix} \begin{bmatrix} a_o \\ a_1 \\ a_2 \\ a_3 \end{bmatrix} \tag{I-14}$$

I-14 in terms of u_2^1, u_6^1, u_2^2, u_6^2, is

$$V_{s_d} = \tfrac{1}{2}SK\begin{bmatrix} u_2^1 & u_6^1 & u_2^2 & u_6^2 \end{bmatrix}\begin{bmatrix} \frac{13}{35}L & \frac{11}{210}L^2 & \frac{9}{70}L & \frac{-13}{420}L^2 \\ \frac{11}{210}L & \frac{1}{105}L^2 & \frac{13}{420}L^2 & \frac{-1}{140}L^3 \\ \frac{9}{70}L & \frac{13}{420}L^2 & \frac{13}{35}L & \frac{-11}{210}L^2 \\ \frac{-13}{420}L^2 & \frac{-1}{140}L^3 & \frac{-11}{210}L^2 & \frac{1}{105}L^3 \end{bmatrix}\begin{bmatrix} u_2^1 \\ u_6^1 \\ u_2^2 \\ u_6^2 \end{bmatrix} \qquad \text{(I-15)}$$

where

$$\begin{bmatrix} a_o \\ a_1 \\ a_2 \\ a_3 \end{bmatrix} = \begin{bmatrix} 1 & 0 & 0 & 0 \\ 0 & 1 & 0 & 0 \\ -3L^{-2} & -2L^{-1} & 3L^{-2} & -L^{-1} \\ 2L^{-3} & L^{-2} & -2L^{-3} & L^{-2} \end{bmatrix}\begin{bmatrix} u_2^1 \\ u_6^1 \\ u_2^2 \\ u_6^2 \end{bmatrix} \qquad \text{(I-16)}$$

in terms of u_1^1, u_2^1, u_6^1, u_1^2, u_2^2, u_6^2 after taking the partial with respect to y yields

$$\underset{\sim}{K}\,\underset{\sim}{u}_d = \begin{bmatrix} 0 & 0 & 0 & 0 & 0 & 0 \\ 0 & \frac{13}{35}SK^*L & \frac{11}{210}SK^*L^2 & 0 & \frac{9}{70}SK^*L & \frac{-13}{420}SK^*L^2 \\ 0 & \frac{11}{210}SK^*L^2 & \frac{1}{105}SK^*L^3 & 0 & \frac{13}{420}SK^*L^2 & \frac{-1}{140}SK^*L^3 \\ 0 & 0 & 0 & 0 & 0 & 0 \\ 0 & \frac{9}{70}SK^*L & \frac{13}{420}SK^*L^2 & 0 & \frac{13}{35}SK^*L & \frac{-11}{210}SK^*L^2 \\ 0 & \frac{-13}{420}SK^*L^2 & \frac{-1}{140}SK^*L^3 & 0 & \frac{-11}{210}SK^*L^2 & \frac{1}{105}SK^*L^3 \end{bmatrix}\begin{bmatrix} u_1^1 \\ u_2^1 \\ u_6^1 \\ u_1^2 \\ u_2^2 \\ u_6^2 \end{bmatrix} \qquad \text{(I-17)}$$

The (6 x 6) matrix is the stiffness matrix for the substrate below a disc element.

The energy stored in the substrate below a differential element of a vertebrae is

$$d\,V_{s_v} = \frac{1}{2}\,SK\,u_2(X_1)^2\,dX_1 \tag{I-18}$$

here $u_2(X_1) = a_0 + a_1X_1$ (rigid body motion only) (I-19)

thus, $$u_2(X_1) = u_2^1 + u_6^1X_1 \tag{I-20}$$

where $u_6^1 = (u_2^2 - u_2^1)/\ell$.

Thus, $$V_{s_v} = \frac{1}{2}\,SK \int_o^{\ell} (u_2^1 + u_6^1X_1)^2 dX_1 \tag{I-21}$$

in quadratic form

$$V_{sv} = \tfrac{1}{2}SK\,[u_1^1\ u_2^1\ u_6^1] \begin{bmatrix} 0 & 0 & 0 \\ 0 & L & L^2/2 \\ 0 & L^2/2 & L^3/3 \end{bmatrix} \begin{bmatrix} u_1^1 \\ u_2^1 \\ u_6^1 \end{bmatrix} \tag{I-22}$$

the resulting $\underset{\sim}{K}_s\ \underset{\sim}{u}_v$ after taking the partial with respect to u is

$$\underset{\sim}{K}_s\,\underset{\sim}{u}_v = SK \begin{bmatrix} 0 & 0 & 0 \\ 0 & L & L^2/2 \\ 0 & L^2/2 & L^3/3 \end{bmatrix} \begin{bmatrix} u_1^1 \\ u_2^1 \\ u_6^1 \end{bmatrix} \tag{I-23}$$

Curved Beam Elements for Ribs

Since the ribs are actually curved beams of three distinct curvatures, a curved finite element was developed. Due to the large radius of curvature and slenderness of the rib sections, a linear stress distribution across the rib can be assumed. As a result of this assumption, the same type of finite element can be used like that used for a straight beam only X_1 is replaced by $\rho\theta$. To clarify this, the strain energy stored in the bending of a straight beam about the major axis is:

$$V = \frac{1}{2}\int_0^{\ell} \frac{M_b^2}{EI_z'}\, dX_1 \qquad \text{(I-24)}$$

For slender beams,

$$\frac{d^2\omega}{dX_1^2} = \frac{M_b}{EI_z} \qquad (M_b \text{ is the bending moment along the beam}) \qquad \text{(I-25)}$$

for the rib case, X_1 would be replaced by $\rho\theta$. Thus rearranging Equation (25) and putting it in terms of $\rho\theta$.

$$M_b = EI_z' \frac{d^2\omega}{d(\rho\theta)^2} \qquad \text{(I-26)}$$

thus Equation 24 becomes

$$V = \frac{1}{2}\int_0^{\beta} \frac{[EI_z'\ d^2\omega/d(\rho\theta)^2]^2}{EI_z'}\, d(\rho\theta) \qquad \text{(I-27)}$$

Since ρ is a constant

$$V = \frac{1}{2} EI_z'\ \rho \int_0^{\beta} [d^2\omega/d(\rho\theta)^2]^2\, d\theta \qquad \text{(I-28)}$$

Again assuming a displacement function that is a function of the form

$$\omega(\rho\theta) = A_o + A_1\rho\theta + A_2(\rho\theta)^2 + A_3(\rho\theta)^3 \qquad \text{(I-29)}$$

gives the same results as that of the disc bending element only ℓ is replaced by $\rho\beta$. Thus for the rib elements, $\underset{\sim}{K}_r \underset{\sim}{u}_r$ in terms of u_1^1, u_2^1, u_3^1, u_4^1, u_5^1, u_6^1, u_1^2, u_2^2, u_3^2, u_4^2, u_5^2, u_6^2 is

$$\underset{\sim}{K}_r \underset{\sim}{u}_r = \begin{bmatrix}
0 & 0 & 0 & 0 & 0 & 0 & 0 & 0 & 0 & 0 & 0 & 0 \\
0 & \frac{12EI'_z}{(\rho\beta)^3} & 0 & 0 & 0 & \frac{6EI'_z}{(\rho\beta)^2} & 0 & \frac{-12EI'_z}{(\rho\beta)^3} & 0 & 0 & 0 & \frac{6EI'_z}{(\rho\beta)^2} \\
0 & 0 & 0 & 0 & 0 & 0 & 0 & 0 & 0 & 0 & 0 & 0 \\
0 & 0 & 0 & 0 & 0 & 0 & 0 & 0 & 0 & 0 & 0 & 0 \\
0 & 0 & 0 & 0 & 0 & 0 & 0 & 0 & 0 & 0 & 0 & 0 \\
0 & \frac{6EI'_z}{(\rho\beta)^2} & 0 & 0 & 0 & \frac{4EI'_z}{(\rho\beta)} & 0 & \frac{-6EI'_z}{(\rho\beta)^2} & 0 & 0 & 0 & \frac{2EI'_z}{(\rho\beta)} \\
0 & 0 & 0 & 0 & 0 & 0 & 0 & 0 & 0 & 0 & 0 & 0 \\
0 & \frac{-12EI'_z}{(\rho\beta)^3} & 0 & 0 & 0 & \frac{-6EI'_z}{(\rho\beta)^2} & 0 & \frac{12EI'_z}{(\rho\beta)^3} & 0 & 0 & 0 & \frac{-6EI'_z}{(\rho\beta)^2} \\
0 & 0 & 0 & 0 & 0 & 0 & 0 & 0 & 0 & 0 & 0 & 0 \\
0 & 0 & 0 & 0 & 0 & 0 & 0 & 0 & 0 & 0 & 0 & 0 \\
0 & 0 & 0 & 0 & 0 & 0 & 0 & 0 & 0 & 0 & 0 & 0 \\
0 & \frac{6EI'_z}{(\rho\beta)^2} & 0 & 0 & 0 & \frac{2EI'_z}{(\rho\beta)} & 0 & \frac{-6EI'_z}{(\rho\beta)^2} & 0 & 0 & 0 & \frac{4EI'_z}{(\rho\beta)}
\end{bmatrix} \begin{bmatrix} u_1^1 \\ u_2^1 \\ u_3^1 \\ u_4^1 \\ u_5^1 \\ u_6^1 \\ u_1^2 \\ u_2^2 \\ u_3^2 \\ u_4^2 \\ u_5^2 \\ u_6^2 \end{bmatrix} \qquad \text{(I-30)}$$

The formulation of the energy stored in the deflected skin of the rib end connected to the sternum and the skin round the head is treated like that of a spring. For the head, which is assumed to pivot with C2 the deflection of the head spring is Equation I-31.

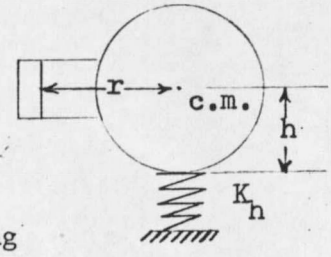


Figure I-3.--Head spring

$$u_h = (u^1_{2_{(C2)}} + r\, u^1_{6_{(C2)}}) \qquad \text{(I-31)}$$

Here u_h is linearized as it stands and is the deflection of the spring perpendicular to the spring.

From the energy equation for a spring $U = \frac{1}{2} K_h u_h^2$, the resulting $\underset{\sim}{K}_h \underset{\sim}{u}_{C(2)}$ is

$$\underset{\sim}{K}_h \underset{\sim}{u}_{C(2)} = \begin{bmatrix} 0 & 0 & 0 \\ 0 & K_h & rK_h \\ 0 & rK_h & r^2K_h \end{bmatrix} \begin{bmatrix} u^1_1 \\ u^1_2 \\ u^1_6 \end{bmatrix} \qquad \text{(I-32)}$$

For the ribs the spring K_r is deflected.

$$u_r = u^2_{2_{r_{(x-3)}}} \cos(\alpha_{x-3}) + u^2_{1_{r_{(x-3)}}} \sin(\alpha_{x-3}) \qquad \text{(I-33)}$$

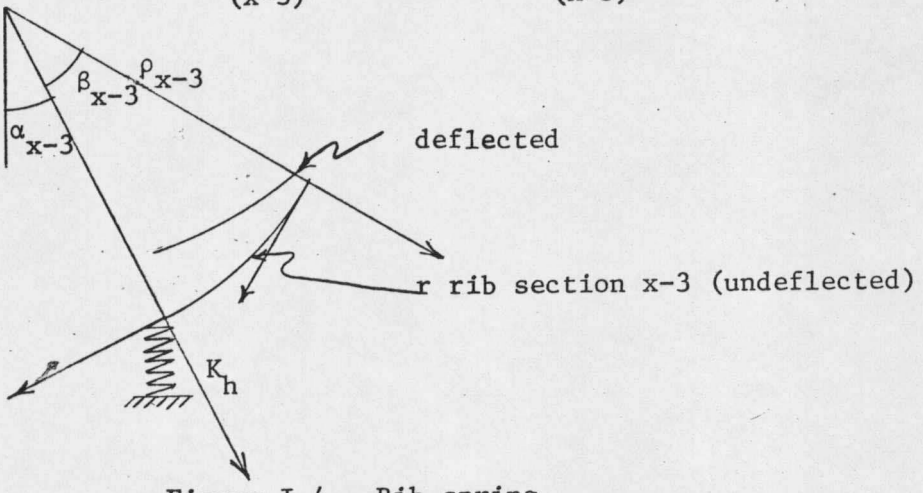


Figure I-4.--Rib spring

The energy stored is $V = \frac{1}{2} K_r (u_r)^2$ results in the following.

$$\underset{\sim}{K}_r \underset{\sim}{u} = K_r \begin{bmatrix} 0 & 0 & 0 & 0 & 0 & 0 & 0 & 0 & 0 & 0 & 0 & 0 \\ 0 & 0 & 0 & 0 & 0 & 0 & 0 & 0 & 0 & 0 & 0 & 0 \\ 0 & 0 & 0 & 0 & 0 & 0 & 0 & 0 & 0 & 0 & 0 & 0 \\ 0 & 0 & 0 & 0 & 0 & 0 & 0 & 0 & 0 & 0 & 0 & 0 \\ 0 & 0 & 0 & 0 & 0 & 0 & 0 & 0 & 0 & 0 & 0 & 0 \\ 0 & 0 & 0 & 0 & 0 & 0 & 0 & 0 & 0 & 0 & 0 & 0 \\ 0 & 0 & 0 & 0 & 0 & 0 & (\sin\alpha)^2 & \sin\alpha\cos\alpha & 0 & 0 & 0 & 0 \\ 0 & 0 & 0 & 0 & 0 & 0 & \sin\alpha\cos\alpha & (\cos\alpha)^2 & 0 & 0 & 0 & 0 \\ 0 & 0 & 0 & 0 & 0 & 0 & 0 & 0 & 0 & 0 & 0 & 0 \\ 0 & 0 & 0 & 0 & 0 & 0 & 0 & 0 & 0 & 0 & 0 & 0 \\ 0 & 0 & 0 & 0 & 0 & 0 & 0 & 0 & 0 & 0 & 0 & 0 \\ 0 & 0 & 0 & 0 & 0 & 0 & 0 & 0 & 0 & 0 & 0 & 0 \end{bmatrix} \begin{bmatrix} u_1 \\ v_1 \\ \theta_1 \\ u_2 \\ v_2 \\ \theta_2 \end{bmatrix} \quad \text{(I-34)}$$

The kinetic energy of the vertebrae is that of a rigid body.

$$T = \frac{1}{2} m_v V_{c.m.}^2 \quad \text{(I-35)}$$

where $V_{c.m.}$ = velocity of the center of mass of the vertebrae. The deflected vertebra is shown below

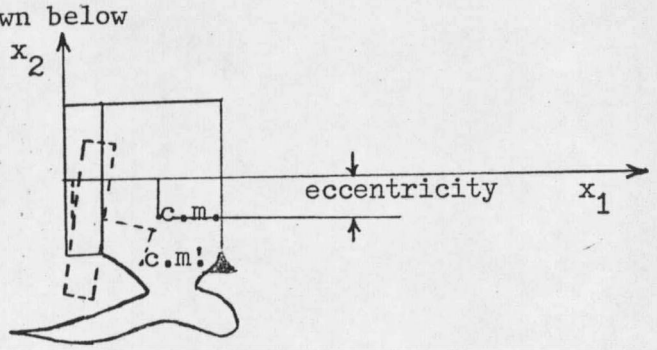


Figure I-5.--Vertebral element

Position vector to c.m.' from the 1st vertebral end linearized is

$$D = (u_1^1 + b/2 + e\ u_6^1)\underline{e}_1 + (u_2^1 + b/2\ \ u_6^2)\ \underline{e}_2 \tag{I-36}$$

Thus $V_{c.m.}$ is

$$V_{c.m.} = \dot{D} = (\dot{u}_1^1 + e\dot{u}_6^1)\underline{e}_1 + (\dot{u}_2^1 + b/2\ \dot{u}_6^2)\underline{e}_2 \tag{I-37}$$

and

$$T = \tfrac{1}{2}M_v \begin{bmatrix} \dot{u}_1^1 & \dot{u}_2^1 & \dot{u}_6^1 \end{bmatrix} \begin{bmatrix} 1 & 0 & e \\ 0 & 1 & b/2 \\ e & b/2 & (e^2+\frac{b^2}{4}) \end{bmatrix} \begin{bmatrix} \dot{u}_1^1 \\ \dot{u}_2^1 \\ \dot{u}_6^1 \end{bmatrix} \tag{I-38}$$

taking $\frac{d}{dt}(\frac{\partial}{\partial y})$ implies $\underset{\sim}{m}_u\ \ddot{\underset{\sim}{u}}$ where

$$\underset{\sim}{M}_v\ddot{\underset{\sim}{u}} = \begin{bmatrix} 1 & 0 & e \\ 0 & 1 & b/2 \\ e & b/2 & (e^2+\frac{b^2}{4}) \end{bmatrix} \begin{bmatrix} \ddot{u}_1^1 \\ \ddot{u}_2^1 \\ \ddot{u}_6^1 \end{bmatrix} \tag{I-39}$$

The kinetic energy of the discs is given by

$$T = \frac{1}{2}\int_o^{\ell} \rho_d[\dot{a}_2(X_1)]^2\ dX_1 \tag{I-40}$$

where ρ_d is the mass/unit length and $\dot{a}_2(X_1)$ is the time derivative of the assumed displacement function. After integration and taking d/dt $(\partial T/\partial \underset{\sim}{u})$ the resulting $\underset{\sim}{m}_D\ddot{\underset{\sim}{u}}_D$ for the disc is

$$\underset{\sim}{m}_d\ddot{\underset{\sim}{u}}_d = \begin{bmatrix} 0 & 0 & 0 & 0 & 0 & 0 \\ 0 & \frac{13}{35}L & \frac{11}{210}L^2 & 0 & \frac{9}{70}L & \frac{-13}{420}L^2 \\ 0 & \frac{11}{210}L^2 & \frac{1}{105}L^3 & 0 & \frac{13}{420}L^2 & \frac{-1}{140}L^3 \\ 0 & 0 & 0 & 0 & 0 & 0 \\ 0 & \frac{9}{70}L & \frac{13}{420}L^2 & 0 & \frac{13}{35}L & \frac{-11}{210}L^2 \\ 0 & \frac{-13}{420}L^2 & \frac{-1}{140}L^3 & 0 & \frac{-11}{210}L^2 & \frac{1}{105}L^3 \end{bmatrix} \begin{bmatrix} \ddot{u}_1^1 \\ \ddot{u}_2^1 \\ \ddot{u}_6^1 \\ \ddot{u}_1^2 \\ \ddot{u}_2^2 \\ \ddot{u}_6^2 \end{bmatrix} \qquad \text{(I-41)}$$

By the same token the same procedure is applied to the assumed displacement function for the ribs resulting in the following.

$$\underset{\sim}{m}_r\ddot{\underset{\sim}{u}}_r = \begin{bmatrix} 0 & 0 & 0 & 0 & 0 & 0 & 0 & 0 & 0 & 0 & 0 & 0 \\ 0 & \frac{13}{35}(\rho\beta) & 0 & 0 & 0 & \frac{11}{210}(\rho\beta)^2 & 0 & \frac{9}{70}(\rho\beta) & 0 & 0 & 0 & \frac{-13}{420}(\rho\beta)^2 \\ 0 & 0 & 0 & 0 & 0 & 0 & 0 & 0 & 0 & 0 & 0 & 0 \\ 0 & 0 & 0 & 0 & 0 & 0 & 0 & 0 & 0 & 0 & 0 & 0 \\ 0 & 0 & 0 & 0 & 0 & 0 & 0 & 0 & 0 & 0 & 0 & 0 \\ 0 & \frac{11}{210}(\rho\beta)^2 & 0 & 0 & 0 & \frac{1}{105}(\rho\beta)^3 & 0 & \frac{13}{420}(\rho\beta)^2 & 0 & 0 & 0 & \frac{-1}{140}(\rho\beta)^3 \\ 0 & 0 & 0 & 0 & 0 & 0 & 0 & 0 & 0 & 0 & 0 & 0 \\ 0 & \frac{9}{70}(\rho\beta) & 0 & 0 & 0 & \frac{13}{420}(\rho\beta)^2 & 0 & \frac{13}{35}(\rho\beta) & 0 & 0 & 0 & \frac{-11}{210}(\rho\beta)^2 \\ 0 & 0 & 0 & 0 & 0 & 0 & 0 & 0 & 0 & 0 & 0 & 0 \\ 0 & 0 & 0 & 0 & 0 & 0 & 0 & 0 & 0 & 0 & 0 & 0 \\ 0 & 0 & 0 & 0 & 0 & 0 & 0 & 0 & 0 & 0 & 0 & 0 \\ 0 & \frac{-13}{420}(\rho\beta)^2 & 0 & 0 & 0 & \frac{-1}{140}(\rho\beta)^3 & 0 & \frac{-11}{210}(\rho\beta)^2 & 0 & 0 & 0 & \frac{1}{105}(\rho\beta)^3 \end{bmatrix} \begin{bmatrix} \ddot{u}_1^1 \\ \ddot{u}_2^1 \\ \ddot{u}_3^1 \\ \ddot{u}_4^1 \\ \ddot{u}_5^1 \\ \ddot{u}_6^1 \\ \ddot{u}_1^2 \\ \ddot{u}_2^2 \\ \ddot{u}_3^2 \\ \ddot{u}_4^2 \\ \ddot{u}_5^2 \\ \ddot{u}_6^2 \end{bmatrix} \qquad \text{(I-42)}$$

The sacral mass is assumed to be triangular shaped such that its center of mass is located one third times the length (L) from the disc below L5. Thus the velocity of the c.m. is

$$V_{c.m.} = \frac{1}{3}\dot{u}_6^1 L \qquad \text{(I-43)}$$

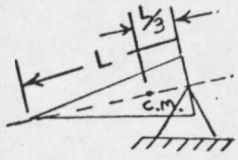


Figure I-6 (sacrum connection)

Thus from $T = \frac{1}{2} m_s (V_{c.m.})^2$ and performing $d/dt(\partial/\partial \underset{\sim}{\dot{u}})$ results with a mass matrix as follows:

$$\underset{\sim}{M}_s \underset{\sim}{\ddot{u}} = \begin{bmatrix} 0 & 0 & 0 & 0 & 0 & 0 \\ 0 & 0 & 0 & 0 & 0 & 0 \\ 0 & 0 & m_s L^2/9 & 0 & 0 & 0 \\ 0 & 0 & 0 & 0 & 0 & 0 \\ 0 & 0 & 0 & 0 & 0 & 0 \\ 0 & 0 & 0 & 0 & 0 & 0 \end{bmatrix} \begin{bmatrix} \ddot{u}^1_1 \\ \ddot{u}^1_{11} \\ \ddot{u}^1_{12} \\ \ddot{u}^1_{16} \\ \ddot{u}^2_{11} \\ \ddot{u}^2_{12} \\ \ddot{u}^2_{22} \\ \ddot{u}^2_{26} \end{bmatrix} \qquad \text{(I-44)}$$

The kinetic energy of the head mass is $T = \frac{1}{2} m_h (V_{c.m.})^2$. The linearized displacement of the center of mass is:

$$D = (u^1_{2(C2)} + r\, u^1_{6(C2)})\underline{e}_2 + u^1_{1(C2)}\, \underline{e}_1 \qquad \text{(I-45)}$$

thus
$$V_{c.m.} = (\dot{u}^1_{2(C2)} + r\, \dot{u}^1_{6(C2)})\underline{e}_2 + \dot{u}^1_{1(C2)}\, \underline{e}_1 \qquad \text{(I-46)}$$

Performing $d/dt\ (\partial T/\partial u)$ yields

$$\underset{\sim}{M}_{hc}\underset{\sim}{u}_{c}(2) = \begin{bmatrix} m_h & 0 & 0 \\ 0 & m_h & rm_h \\ 0 & rm_h & r^2 m_h \end{bmatrix} \begin{bmatrix} u_1^1 \\ u_2^1 \\ u_6^1 \end{bmatrix} \qquad \text{(I-47)}$$

All of the mass and stiffness matrices have now been developed.

Transformation Matrices for Straight Beams

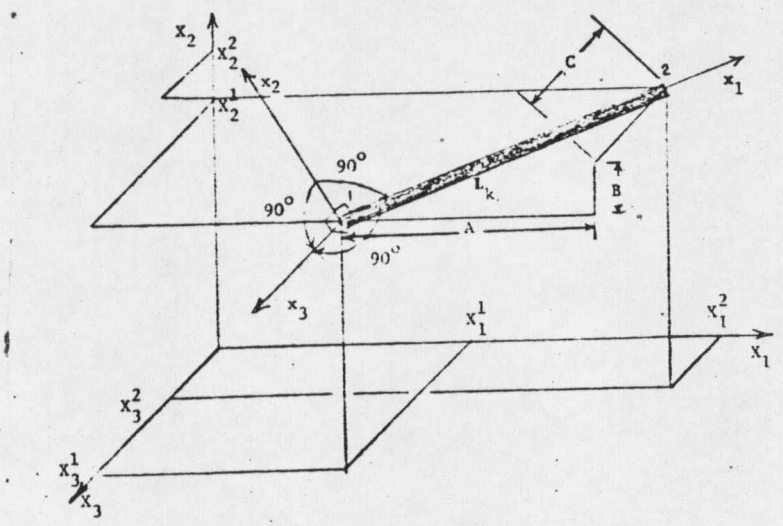


Figure I-7.--Straight beam element

For any straight beam element, the X_1 direction coincides with the length of the element. For the vertebral system, the x_3 direction is parallel to the X_3 direction. Thus the x_3 coordinate direction can be obtained by crossing the x_1 coordinate vector with the component of the x_1 coordinate vector in the X_1X_3 plane. The x_2 coordinate direction is merely the cross product of the x_3 coordinate direction with the x_1 coordinate. Thus, the coordinate directions expressed in the global coordinate system are

$$\underline{e}_1 = \frac{A}{k}\underline{i} + \frac{B}{k}\underline{j} + \frac{C}{k}\underline{K} \tag{I-48}$$

$$\underline{e}_3 = \frac{(A\,\underline{i} + C\,\underline{K}) \times (A\,\underline{i} + B\,\underline{i} + C\,\underline{K})}{\left|\left|(A\,\underline{i} + C\,\underline{K}) \times (A\,\underline{i} + B\,\underline{i} + C\,\underline{K})\right|\right|} \tag{I-49}$$

$$\underline{e}_2 = \underline{e}_3 \times \underline{e}_1 \tag{I-50}$$

The resulting transformation matrix for straight beams is

$$\underset{\sim}{T} = \begin{bmatrix} \frac{A}{L_k} & \frac{B}{L_k} & \frac{C}{L_k} \\ \frac{-AB}{L_{1k}} & \frac{(A^2+C^2)}{L_{1k}} & \frac{-CB}{L_{1k}} \\ \frac{-C}{L_{2k}} & 0 & \frac{A}{L_{2k}} \end{bmatrix} \tag{I-51}$$

where $L_k = (A^2 + B^2 + C^2)^{1/2}$

$L_{1k} = (A^2B^2 + A^4 + 2A^2C^2 + C^4 + C^2B^2)^{1/2}$

$L_{2k} = (C^2 + A^2)^{1/2}$

For the three degrees of freedom vertebral elemental matrix the transformation matrix is $\underset{\sim}{T}$. For the six degrees of freedom intervertebral disc elemental matrix the transformation matrix is shown below.

$$\underset{\sim}{T}(\text{disc}) = \begin{bmatrix} \underset{\sim}{T} & \underset{\sim}{0} \\ \underset{\sim}{0} & \underset{\sim}{T} \end{bmatrix} \qquad \text{(I-52)}$$

This type of transformation matrix is appropriate for any case where the minor axis vector of the element is perpendicular to the X_2 axis.

Transformation Matrices for Curved Beams

Unlike a straight beam element, the end one coordinate directions are not the same as the end two directions. This is shown in Figure I-8.

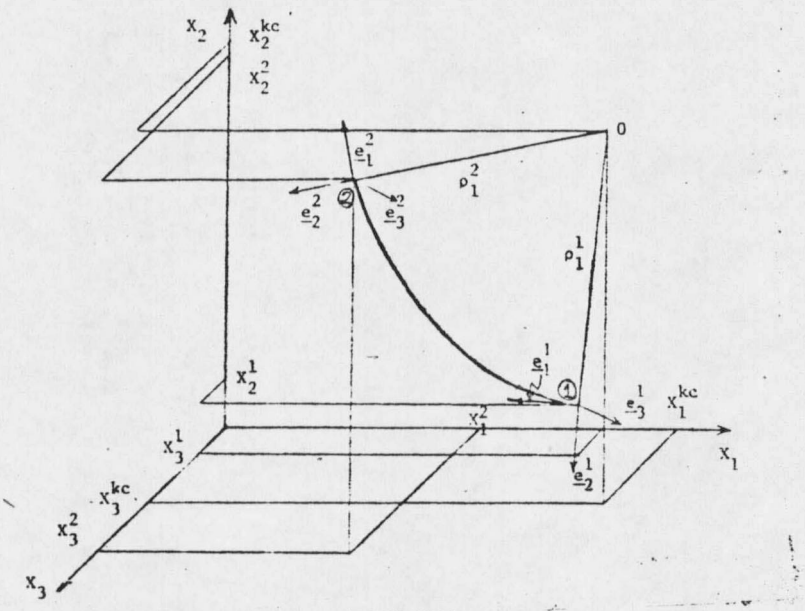


Figure I-8.--Curved beam element

In terms of the global coordinates system, $\underline{\rho}_1^1$ and $\underline{\rho}_1^2$ are

$$\underline{\rho}_1^1 = (X_1^1 - X_1^{kc})\ \underline{i} + (X_2^1 - X_2^{kc})\ \underline{j} + (X_3^1 - X_3^{kc})\ \underline{k} \qquad \text{(I-53)}$$

$$= A\ \underline{i} + b\ \underline{j} + C\ \underline{K}$$

$$\underline{\rho}_1^2 = (X_1^2 - X_1^{kc})\ \underline{i} + (X_2^2 - X_1^{kc})\ \underline{j} + (X_3^2 - X_3^{kc})\ \underline{k} \qquad \text{(I-54)}$$

$$= D\ \underline{i} + E\ \underline{j} + F\ \underline{K}$$

From Figure I-8, it is apparent that the $\underline{e}_2^2$ vector is parallel to the $\underline{\rho}_1^2$ vector and the $\underline{e}_2^1$ vector is parallel to the $\underline{\rho}_1^1$ vector. Thus the $\underline{e}_2^1$ and $\underline{e}_2^2$ vectors are

$$\underline{e}_2^1 = \frac{A}{||\rho_1^1||}\underline{i} + \frac{B}{||\rho_1^1||}\underline{j} + \frac{C}{||\rho_1^1||}\underline{K} \tag{I-55}$$

$$\underline{e}_2^2 = \frac{D}{||\rho_1^1||}\underline{i} + \frac{E}{||\rho_1^1||}\underline{j} + \frac{F}{||\rho_1^1||}\underline{K} \tag{I-56}$$

The cross-product between $\underline{\rho}_1^2$ and $\underline{\rho}_1^2$ is in the elemental x_3 direction for both end 1 and end 2. The resulting $\underline{e}_3^1$ and $\underline{e}_3^2$ vectors are

$$\underline{e}_3^1 = \underline{e}_3^2 = \frac{(\rho_1^2 \times \rho_1^1)}{||\rho_1^2 \times \rho_1^1||} \tag{I-57}$$

The remaining $\underline{e}_1$ vectors can be attained by the cross-product of the $\underline{e}_2$ and $\underline{e}_3$ vectors. The resulting transformation matrix for the rib curved elements is thus

$$\underset{\sim}{T}_R = \begin{bmatrix} R_1 & 0 & 0 & 0 \\ 0 & R_1 & 0 & 0 \\ 0 & 0 & R_2 & 0 \\ 0 & 0 & 0 & R_2 \end{bmatrix} \tag{I-58}$$

where

$$R_1 = \begin{bmatrix} \frac{(C^2D-ACF-ABE+B^2D)}{||\rho_1^1\times(\rho_1^2\times\rho_1^1)||} & \frac{(-BCF+C^2E+A^2E-ABD)}{||\rho_1^1\times(\rho_1^2\times\rho_1^1)||} & \frac{(B^2F-BCE-ACD+A^2F)}{||\rho_1^1\times(\rho_1^2\times\rho_1^1)||} \\ \frac{A}{||\rho_1^1||} & \frac{B}{||\rho_1^1||} & \frac{C}{||\rho_1^1||} \\ \frac{(-BF+CE)}{||\rho_1^2\times\rho_1^1||} & \frac{(-CD+AF)}{||\rho_1^2\times\rho_1^1||} & \frac{(-AE+BD)}{||\rho_1^2\times\rho_1^1||} \end{bmatrix}$$

$$R_2 = \begin{bmatrix} \frac{(CDF-AF^2-AE^2+BDE)}{||\rho_1^1\times(\rho_1^2\times\rho_1^1)||} & \frac{(-BF^2+CEF+ADE-BD^2)}{||\rho_1^1\times(\rho_1^2\times\rho_1^1)||} & \frac{(BEF-CE^2-CD^2+ADF)}{||\rho_1^1\times(\rho_1^2\times\rho_1^1)||} \\ \frac{D}{||\rho_1^2||} & \frac{E}{||\rho_1^2||} & \frac{F}{||\rho_1^2||} \\ \frac{(-BF+CE)}{||\rho_1^2\times\rho_1^1||} & \frac{(-CD+AF)}{||\rho_1^2\times\rho_1^1||} & \frac{(-AE+BD)}{||\rho_1^2\times\rho_1^1||} \end{bmatrix}$$

Transformation of End Two Vertebral Displacements to End One Vertebral Displacements

Once the elemental matrices are transformed to global coordinates, the end one displacements of the intervertebral discs and rib elements directly connected to the vertebrae must be transformed to end one displacements of the vertebrae. This is due to the fact that the vertebrae are rigid bodies and their motion is described in terms of the end one displacements. The end two displacements in terms of end one displacements for small displacements are

$$u_1^2 = u_1^1 \tag{I-59}$$

$$u_2^2 = u_2^1 + Lu_6^1 \tag{I-60}$$

$$u_6^2 = u_6^1 \tag{I-61}$$

where L = length of vertebra.

Thus in matrix form

$$\begin{bmatrix} U_1^2 \\ U_2^2 \\ U_6^2 \end{bmatrix} = \begin{bmatrix} 1 & 0 & 0 \\ 0 & 1 & L \\ 0 & 0 & 1 \end{bmatrix} \begin{bmatrix} U_1^1 \\ U_2^1 \\ U_6^1 \end{bmatrix} \tag{I-62}$$

The entire transformation matrix for the intervertebral disc elements would be a 6 x 6 matrix with ones on the diagonal and the row 2 column 3 position containing L. For the first rib section connecting to the vertebra, the elemental matrix when transferred to the global coordinates is reduced to a 11 x 11 matrix by the elimination of the row and column associated with X_3 displacement of the first end. Thus, the rib transformation matrix for end two displacements to end one is a 11 x 11 matrix with ones along the diagonal and an L in the row 2 column 3 position.

APPENDIX II

ANTHROPOMETRIC DATA

Global Coordinates

The following set of data in Table II-1 is the global coordinates of each element in the model. The notation Xij refers to the ith direction where i = 1, 2, or 3 and j refers to end 1 or 2 of the element. The notation DBXXX refers to the intervertebral disc below vertebra XXX. L5-L1 refers to the lumbar vertebrae, T12-T1 refers to the thoracic vertebrae, and C7-C2 refers to the cervical vertebrae.

Table II-1.--Global Coordinates

Element	X11 (in.)	X21 (in.)	X31 (in.)	X12 (in.)	X22 (in.)	X32 (in.)
DBL5	0.00	0.00	0.00	0.56	0.26	0.00
L5	0.56	0.26	0.00	1.58	0.48	0.00
DBL4	1.58	0.48	0.00	2.16	0.50	0.00
L4	2.16	0.50	0.00	3.22	0.46	0.00
DBL3	3.22	0.46	0.00	3.70	0.45	0.00
L3	3.70	0.45	0.00	4.80	0.36	0.00
DBL2	4.80	0.36	0.00	5.24	0.28	0.00
L2	5.24	0.28	0.00	6.26	0.00	0.00
DBL1	6.26	0.00	0.00	6.68	-0.13	0.00
L1	6.68	-0.13	0.00	7.68	-0.48	0.00
DBT12	7.68	-0.48	0.00	8.00	-0.60	0.00
T12	8.00	-0.60	0.00	8.94	-0.96	0.00
DBT11	8.94	-0.96	0.00	9.20	-1.04	0.00
T11	9.20	-1.04	0.00	10.11	-1.32	0.00
DBT10	10.11	-1.32	0.00	10.32	-1.36	0.00
T10	10.32	-1.36	0.00	11.20	-1.52	0.00
Rib 10-1	11.20	-1.52	0.60	11.06	-1.23	2.07
Rib 10-2	11.06	-1.23	2.07	7.65	6.09	1.51
Rib 10-3	7.65	6.09	1.51	7.57	6.27	0.60
DBT9	11.20	-1.52	0.00	11.39	-1.54	0.00
T9	11.39	-1.54	0.00	12.21	-1.61	0.00
Rib 9-1	12.21	-1.61	0.58	12.10	-1.37	2.19
Rib 9-2	12.10	-1.37	2.19	8.48	6.39	1.94
Rib 9-3	8.48	6.39	1.94	8.20	6.99	0.58
DBT8	12.21	-1.61	0.00	12.39	-1.64	0.00
T8	12.39	-1.64	0.00	13.21	-1.66	0.00

Table II-1.--Continued

Element	X11 (in.)	X21 (in.)	X31 (in.)	X12 (in.)	X22 (in.)	X32 (in.)
Rib 8-1	13.21	-1.66	0.60	13.00	-1.21	2.67
Rib 8-2	13.00	-1.21	2.67	9.46	6.38	2.23
Rib 8-3	9.46	6.38	2.23	9.22	6.89	0.60
DBT7	13.21	-1.66	0.00	13.37	-1.66	0.00
T7	13.37	-1.66	0.00	14.17	-1.68	0.00
Rib 7-1	14.17	-1.68	0.58	13.88	-1.05	2.84
Rib 7-2	13.88	-1.05	2.84	10.48	6.22	1.91
Rib 7-3	10.48	6.22	1.91	10.30	6.61	0.58
DBT6	14.17	-1.68	0.00	14.30	-1.65	0.00
T6	14.30	-1.65	0.00	15.06	-1.50	0.00
Rib 6-1	15.06	-1.50	0.56	14.69	-0.71	2.97
Rib 6-2	14.69	-0.71	2.97	11.46	6.23	1.74
Rib 6-3	11.46	6.23	1.74	11.34	6.48	0.56
DBT5	15.06	-1.50	0.00	15.18	-1.46	0.00
T5	15.18	-1.46	0.00	15.90	-1.24	0.00
Rib 5-1	15.90	-1.24	0.55	15.61	-0.61	3.30
Rib 5-2	15.61	-0.61	3.30	12.73	5.55	1.76
Rib 5-3	12.73	5.55	1.76	12.57	5.91	0.55
DBT4	15.90	-1.24	0.00	15.98	-1.24	0.00
T4	15.98	-1.22	0.00	16.65	-0.98	0.00
Rib 4-1	16.65	-0.98	0.53	16.42	-0.49	3.41
Rib 4-2	16.42	-0.49	3.41	14.14	4.41	2.11
Rib 4-3	14.14	4.41	2.11	13.72	5.31	0.53
DBT3	16.65	-0.98	0.00	16.77	-0.96	0.00
T3	16.77	-0.96	0.00	17.44	-0.71	0.00
Rib 3-1	17.44	-0.71	0.58	17.03	0.17	3.47
Rib 3-2	17.03	0.17	3.47	15.18	4.13	1.45
Rib 3-3	15.18	4.13	1.45	15.00	4.53	0.58
DBT2	17.44	-0.71	0.00	17.57	-0.66	0.00
T2	17.57	-0.66	0.00	18.22	-0.41	0.00
Rib 2-1	18.32	-0.41	0.52	17.63	0.86	2.78
Rib 2-2	17.63	0.86	2.78	16.36	3.57	0.91
Rib 2-3	16.36	3.57	0.91	16.29	3.72	0.52
DBT1	18.22	-0.41	0.00	18.38	-0.34	0.00
T1	18.38	-0.34	0.00	18.98	0.00	0.00
Rib 1-1	18.98	0.00	0.54	18.51	1.01	2.42
Rib 1-2	18.51	1.01	2.42	17.49	3.20	1.36
Rib 1-3	17.49	3.20	1.36	17.44	3.31	0.54
DBC7	18.98	0.00	0.00	19.06	0.07	0.00
C7	19.06	0.07	0.00	19.51	0.31	0.00
DBC6	19.51	0.31	0.00	19.69	0.40	0.00
C6	19.69	0.40	0.00	20.08	0.58	0.00

Table II-1.--Continued

Element	X11 (in.)	X21 (in.)	X31 (in.)	X12 (in.)	X22 (in.)	X32 (in.)
DBC5	20.08	0.58	0.00	20.25	0.62	0.00
C5	20.25	0.62	0.00	20.63	0.72	0.00
DBC4	20.63	0.72	0.00	20.83	0.76	0.00
C4	20.83	0.76	0.00	21.22	0.78	0.00
DBC3	21.22	0.78	0.00	21.36	0.78	0.00
C3	21.36	0.78	0.00	21.76	0.78	0.00
DBC2	21.76	0.78	0.00	21.88	0.78	0.00
C2	21.88	0.78	0.00	23.22	0.63	0.00

Table II-2.--Global Coordinates of Centers of Curvature for Rib Elements

Rib Section	X1 (in.)	X2 (in.)	X3 (in.)
Rib 10-1	9.73	1.64	0.60
Rib 10-2	9.46	2.21	-1.45
Rib 10-3	11.20	-1.52	-0.83
Rib 9-1	10.21	2.67	0.58
Rib 9-2	10.34	2.40	-2.58
Rib 9-3	12.21	-1.61	-3.16
Rib 8-1	11.25	2.55	0.60
Rib 8-2	11.37	2.29	-2.99
Rib 8-3	13.21	-1.66	-1.71
Rib 7-1	12.46	2.00	0.58
Rib 7-2	12.46	1.99	-3.26
Rib 7-3	14.17	-1.68	-1.62
Rib 6-1	13.44	1.98	0.56
Rib 6-2	13.48	1.88	-3.52
Rib 6-3	15.06	-1.50	-0.79
Rib 5-1	13.49	3.93	0.55
Rib 5-2	14.59	1.57	-1.91
Rib 5-3	15.90	-1.24	-1.34
Rib 4-1	13.07	6.69	0.53
Rib 4-2	15.61	1.26	-0.30
Rib 4-3	16.65	-0.98	-2.71
Rib 3-1	15.38	3.71	0.58
Rib 3-2	16.81	0.64	-1.01
Rib 3-3	17.44	-0.71	-1.81
Rib 2-1	17.12	1.94	0.52
Rib 2-2	18.01	0 04	-1.82
Rib 2-3	18.22	-0.41	-1.32

Table II-2.--Continued

Rib Section	X1 (in.)	X2 (in.)	X3 (in.)
Rib 1-1	18.04	2.02	0.54
Rib 1-2	18.81	0.36	-1.32
Rib 1-3	18.98	0.00	-1.22

Table II-3.--Intervertebral Disc Data Used

Inter-vertebral Disc	Cross-Sectional Type	Moment of Inertia ($in.^4$)	Area (in^2)	Height (in)	Volume (in^3)	Mass (#m/in)
DBL5	ellipse	0.182	1.81	0.618	1.122	0.0063
DBL4	ellips	0.182	1.81	0.551	0.996	0.0064
DBL3	ellipse	0.232	2.00	0.480	0.960	0.0071
DBL2	ellipse	0.192	1.79	0.449	0.806	0.0062
DBL1	ellipse	0.168	1.67	0.394	0.651	0.0059
DBT12	ellipse	0.144	1.53	0.331	0.505	0.0055
DBT11	ellipse	0.126	1.38	0.268	0.373	0.0048
DBT10	ellipse	0.103	1.21	0.201	0.242	0.0048
DBT9	ellipse	0.087	1.07	0.185	0.203	0.0037
DBT8	circular	0.078	1.01	0.177	0.181	0.0036
DBT7	circular	0.078	1.04	0.157	0.166	0.0037
DBT6	circular	0.064	0.95	0.126	0.123	0.0034
DBT5	circular	0.053	0.87	0.102	0.087	0.0031
DBT4	circular	0.038	0.77	0.087	0.069	0.0027
DBT3	circular	0.039	0.76	0.106	0.083	0.0025
DBT2	triangular	0.024	0.68	0.122	0.081	0.0023
DBT1	ellipse	0.0018	0.58	0.177	0.104	0.0021
DBC7	ellipse	0.013	0.52	0.120	0.063	0.0018
DBC6	ellipse	0.014	0.59	0.200	0.119	0.0021
DBC5	ellipse	0.016	0.55	0.160	0.087	0.0019
DBC4	ellipse	0.012	0.46	0.200	0.092	0.0017
DBC3	ellipse	0.012	0.46	0.140	0.064	0.0016
DBC2	ellipse	0.011	0.44	0.120	0.053	0.0015

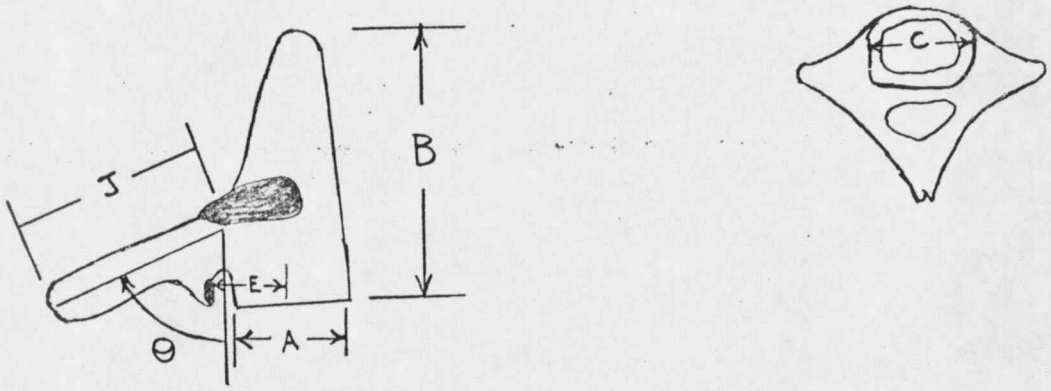


Figure II-1.--Second cervical measurements

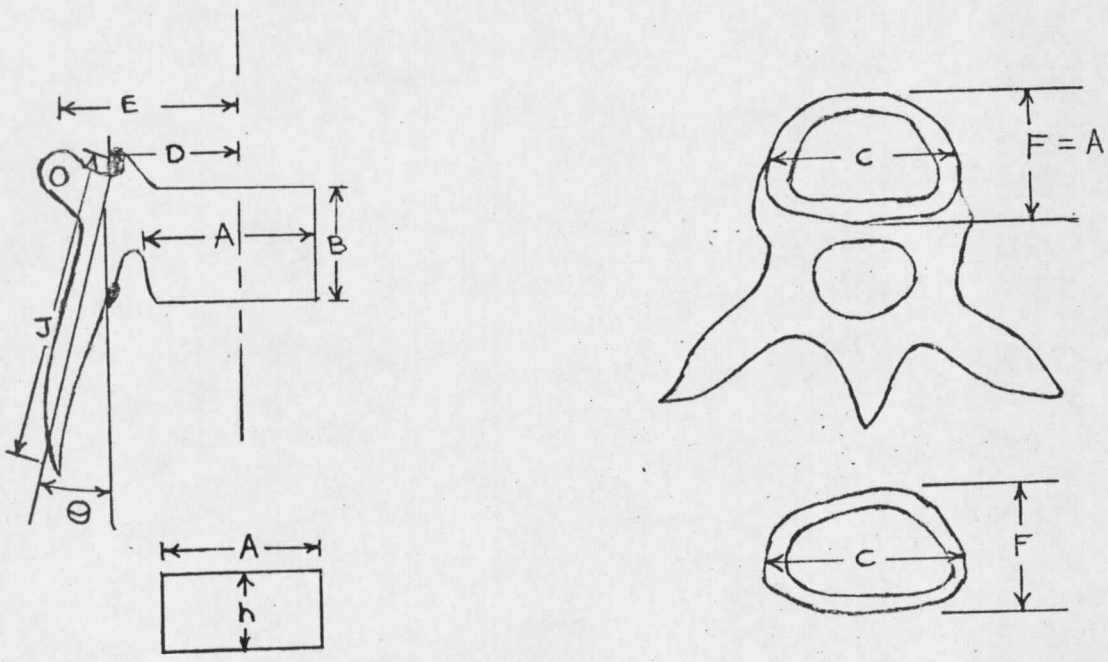


Figure II-2.--Vertebrae and intervertebral disc measurements

Table II-4.--Vertebral Dimensions
See Figure II-1 for Nomenclature on C2

Vertebra	θ	A	B	C	D	E	J
L5	90	1.27	0.90	1.81-E	1.07	0.98	0.67
L4	90	1.36	0.83	1.88-E	1.10	1.31	1.09
L3	90	1.31	0.93	1.74-E	1.46	1.55	1.04
L2	80	1.27	0.93	1.67-E	1.02	1.53	1.28
L1	75	1.23	0.90	1.58-E	1.16	1.37	0.99
T12	70	1.21	0.87	1.45-E	1.16	1.38	0.87
T11	70	1.17	0.83	1.32-E	1.13	1.36	0.93
T10	65	1.14	0.78	1.20-E	1.03	1.30	1.08
T9	45	1.11	0.72	1.16-C	1.06	1.29	1.25
T8	30	1.10	0.67	1.20-C	0.98	1.22	1.38
T7	20	1.04	0.59	1.16-C	0.97	1.13	1.44
T6	15	0.99	0.64	1.12-C	0.88	1.05	1.65
T5	15	0.89	0.62	1.10-C	0.79	0.94	1.47
T4	15	0.91	0.57	1.06-C	0.77	0.87	1.40
T3	20	0.75	0.57	1.15-T	0.76	0.87	1.35
T2	20	0.71	0.56	1.04-E	0.67	0.84	1.36
T1	30	0.62	0.56	1.07-E	0.63	0.69	1.28
C7	30	0.61	0.58	1.24-E	0.55	0.75	1.23
C6	30	0.68	0.51	1.02-E	0.41	0.64	1.25
C5	30	0.65	0.40	0.90-E	0.50	0.59	0.95
C4	40	0.65	0.40	0.90-E	0.41	0.58	0.75
C3	45	0.63	0.40	0.89-E	0.40	0.53	0.72
C2	60	0.65	1.36	0.68	----	0.33	0.63

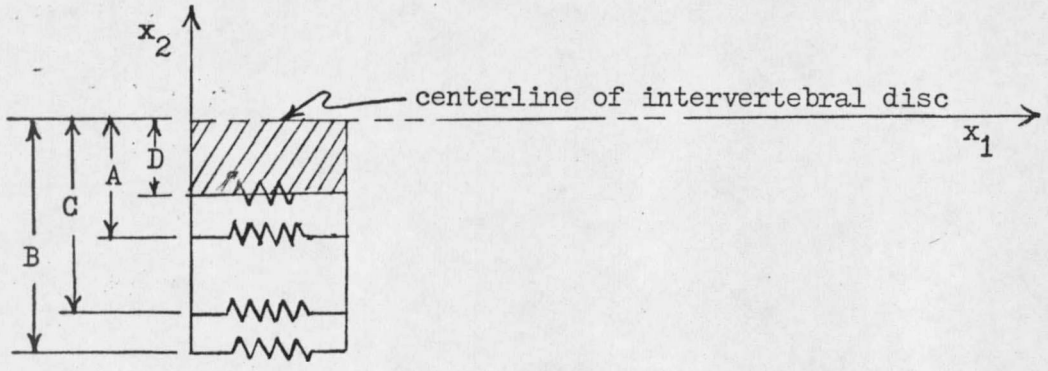


Figure II-3.--Lever arms used for the various ligaments, muscles, and fusions. D is the lever used for a spinal fusion spring, A is the lever arm used for the inferior superior process connective tissue spring, C is the lever arm used for the transverse process muscle connection spring, and B is the level arm used for the spinal process connection spring.

Table II-5.--Spring Lever Arm Lengths in Inches

Element	A (in.)	B (in.)	C (in.)	D (in.)
DBL5	0.82	1.48	0.98	0.50
DBL4	1.09	1.97	1.31	0.66
DBL3	1.28	2.35	1.55	0.67
DBL2	1.24	2.40	1.53	0.65
DBL1	1.09	2.20	1.37	0.63
DBT12	1.16	2.05	1.38	0.61
DBT11	1.15	2.00	1.36	0.60
DBT10	1.08	1.97	1.30	0.58
DBT9	1.05	2.00	1.29	0.56
DBT8	1.02	1.82	1.22	0.55
DBT7	0.98	1.58	1.13	0.54
DBT6	0.93	1.39	1.05	0.51
DBT5	0.84	1.24	0.94	0.47
DBT4	0.78	1.15	0.87	0.45
DBT3	0.77	1.18	0.87	0.42
DBT2	0.72	1.18	0.84	0.37
DBT1	0.65	1.21	0.79	0.33
DBC7	0.59	1.22	0.75	0.31
DBC6	0.48	1.10	0.64	0.32
DBC5	0.46	0.96	0.59	0.33
DBC4	0.46	0.95	0.58	0.33
DBC3	0.41	0.91	0.53	0.32
DBC2	0.20	0.74	0.33	0.32

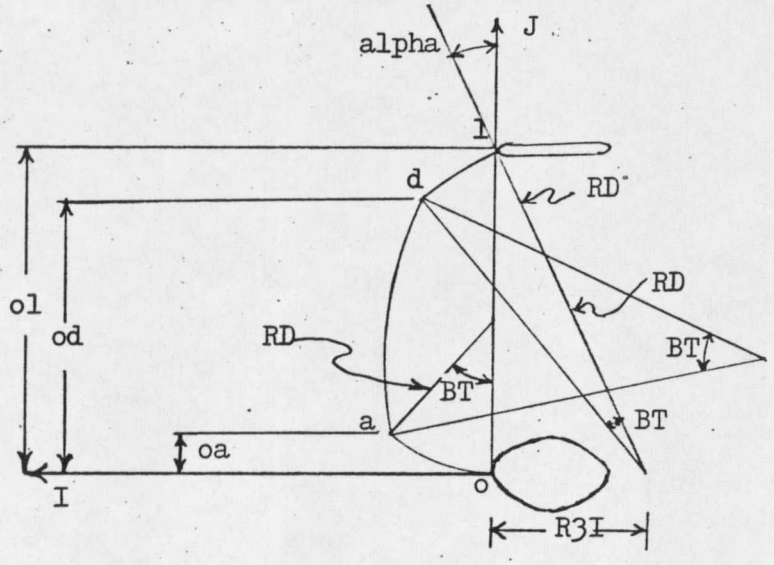


Figure II-4.--Rib Geometry

Table II-6.--Vertebral Data *(The length and width of C1 are incorporated in C2 since C1 is an extension of C2.)

Element	Mass (#m)	Length (in)	Eccentricity (in)	Body Width (in)
L5	0.269	1.04	1.50	1.81
L4	0.288	1.08	1.50	1.88
L3	0.273	1.10	1.50	1.74
L2	0.269	1.10	1.50	1.67
L1	0.257	1.07	1.50	1.58
T12	0.247	1.01	1.50	1.45
T11	0.226	0.96	1.50	1.32
T10	0.201	0.91	1.50	1.20
T9	0.167	0.84	1.50	1.16
T8	0.165	0.82	1.50	1.20
T7	0.169	0.80	1.50	1.16
T6	0.178	0.78	1.50	1.12
T5	0.155	0.77	1.50	1.10
T4	0.152	0.75	1.50	1.06
T3	0.148	0.73	1.50	1.15
T2	0.156	0.71	1.50	1.04
T1	0.140	0.66	0.67	1.07
C7	0.134	0.51	0.67	1.12
C6	0.115	0.44	0.67	0.98
C5	0.119	0.40	0.67	0.90
C4	0.120	0.40	0.67	0.90
C3	0.111	0.40	0.67	0.89
C2	0.141	1.36	0.67	0.68
*C1	0.111	0.00	0.67	0.00

Table II-7.--Rib Data

Rib	Alpha	OA	OD	OL	R3I
10	0.16406	0.402	8.402	8.602	-1.425
9	0.37525	0.263	8.831	9.488	-3.736
8	0.24086	0.504	8.866	9.425	-2.315
7	0.23562	0.685	8.724	9.150	-2.197
6	0.15184	0.866	8.531	8.795	-1.346
5	0.23562	0.705	7.492	7.886	-1.894
4	0.43633	0.543	5.953	6.941	-3.236
3	0.39270	0.972	5.339	5.783	-2.394
2	0.38397	1.398	4.387	4.563	-1.843
1	0.44855	1.110	3.528	3.654	-1.760

Table II-8.--Rib Section Data

Rib Section	Mass (#m/in)	Moment of Inertia (in^4)	Radius (in)	BT (Radians)
10-1	0.00895	0.000794	3.48	0.436
10-2	0.00836	0.000246	5.17	1.789
10-3	0.00523	0.000123	8.72	0.106
9-1	0.00836	0.000741	4.72	0.346
9-2	0.00894	0.000263	6.37	1.495
9-3	0.00452	0.000083	10.20	0.148
8-1	0.00856	0.000759	4.65	0.463
8-2	0.01146	0.000583	6.89	1.305
8-3	0.00736	0.000240	9.70	0.178
7-1	0.00895	0.000794	4.06	0.592
7-2	0.01274	0.001062	7.02	1.225
7-3	0.01086	0.000509	9.41	0.148
6-1	0.00955	0.000847	3.84	0.681
6-2	0.01128	0.001061	7.15	1.146
6-3	0.01158	0.000848	8.90	0.136
5-1	0.00902	0.000849	5.71	0.503
5-2	0.00979	0.000625	5.72	1.300
5-3	0.01042	0.000618	8.11	0.157
4-1	0.00695	0.000579	8.46	0.349
4-2	0.00945	0.000560	4.28	1.453
4-3	0.00803	0.000236	7.66	0.244
3-1	0.00748	0.000585	4.88	0.637
3-2	0.00814	0.000414	4.56	1.104
3-3	0.00912	0.000327	6.26	0.157
2-1	0.00781	0.000779	2.60	1.082
2-2	0.01172	0.000802	4.82	0.755
2-3	0.00637	0.000251	4.92	0.087
1-1	0.00471	0.000153	2.22	1.035
1-2	0.00985	0.000424	3.83	0.599
1-3	0.00985	0.000424	4.06	0.241

APPENDIX III

PROBLEMS ARISING USING THE SWEEPING MATRIX TECHNIQUE SOLUTION

For the vertebral column system with the inclusion of ribs, natural frequencies can result that involve either vertebral motion, rib motion, or a combination of both vertebral and rib motion. When this happens, the natural frequency associated with one type of motion can be close to another natural frequency of another type motion. The sweeping matrix technique is dependent on the fact that the natural frequencies of a system are distinct and well spaced. Therefore, when two natural frequencies are approximately the same, this technique of solution may iterate between the two natural frequencies and never converge to a solution. This became a problem when stiffness parameters for the ribs and the vertebral column were changed. When the intervertebral disc modulus of elasticity value was left the same, cross overs in natural frequencies associated with vertebral motion and rib motion occurred. If the two natural frequencies were virtually the same, no solution was obtained for those natural frequencies as well as the higher natural frequencies above them. The lower natural frequencies below the two that coincided were attained in the solution. To compensate for this problem, the stiffness parameters were varied in the vicinity of the unsolvable stiffness parameter values. The solution for the unsolvable stiffness parameters was then interpolated from those results.

REFERENCES

1. Garner, E. R., and D. O. Blackketter, "In-Vivo Deformation of Macroscopic Biological Material Properties," Journal of Engineering Materials and Technology, Vol. 97, 1975, pp. 350-356.
2. Latham, F., "A Study of Body Ballistics: Seat Ejections," Proc. R. Soc., B-147, 1957, pp. 121-139.
3. Hess, J. L., and C. F. Lombard, "Theoretical Investigations of Dynamic Response of Man to High Vertical Accelerations," J. Aviat. Med., 29, 1958, pp. 66-74.
4. Terry, C. T., and V. L. Roberts, "A Viscoelastic Model of the Human Spine Subjected to $+G_2$ Accelerations," Journal of Biomechanics 1, 1968, pp. 161-168.
5. Orne, D., and Y. K. Liu, "A Mathematical Model of Spinal Response to Impact," Journal of Biomechanics, Vol. 4, 1971, pp. 49-71.
6. Andrracchi, T., A. Schultz, T. Belytschko, and J. Galante, "A Model for Studies of Interactions Between the Human Spine Structure," Journal of Biomechanics, Vol. 7, 1973, pp. 497-507.
7. Jurist, J., "Measurement of Ulnar Resonant Frequency," Orthopedic Research Laboratory, Internal Report No. 36, University of Wisconsin Medical Center, Madison, Wisconsin.
8. Matz, R. E., "Parameter Investigation for Low Frequency Vibration of the Forearm," Master's Thesis, Montana State University, March 1977.

9. Mozer, C. J., "Dynamic Testing as a Diagnostic Technique in Orthopedics," Master's Thesis, Montana State University, December 1974.

10. Harrigan, M. D., "Development of Equipment and Techniques for Experimental Determination of Dynamic Response of the Human Forearm," Master's Thesis, Montana State University, August 1974.

11. Jurist, J., and D. O. Blackketter, "Noninvasive Studies of Skeletal Status," Grant Application to Department of Health, Education and Welfare, 1977.

12. Adelsbach, J. A., "An Analytic Model of the Human Spine under Harmonic Excitation," Master's Thesis, California Polytechnic State University, January 1976.

13. Schultz, A. B., D. R. Benson, and C. Hirsch, "Force-Deformation Properties of Human Ribs," Journal of Biomechanics, Vol. 7, 1974, pp. 303-309.

14. Schultz, A. B., T. B. Belytschko, J. O. Galante, and T. P. Andriacchi, "Analog Studies of Forces in the Human Spine: Mechanical Properties and Motion Segment Behavior," Journal of Biomechanics, Vol. 6, 1973, pp. 373-383.

15. Spiegl, P. V., and J. M. Jurist, "Measurement of Ulnar Resonant Frequency," Orthopedic Research Laboratory, University of Wisconsin Medical Center, Madison, Wisconsin.

16. Grammens, G. M., "Frequency Response Analysis of the In-Vivo Human Skull," Master's Thesis, Montana State University, March 1977.

17. Nickell, R. E., and P. V. Marcal, "In-Vacuo Modal Dynamic Response of the Human Skull," Journal of Engineering for Industry, Vol. 96, 1974, pp. 490-494.

18. Krogman, W. M., The Human Skeleton in Forensic Medicine, Charles C. Thomas Publisher, Springfield, Illinois.

19. Anderson, R. A., Fundamentals of Vibrations, New York: Macmillan, 1967.

20. Meirovitch, L., Analytical Methods in Vibrations, New York: Macmillan, 1967.

21. Evans, G. F., and H. R. Lissner, "Biomechanical Studies on the Lumbar Spine and Pelvis," J. Bone JT Surg., 41-A, 1959, pp. 278-290.

22. Przemieniecki, J. S., Theory of Matrix Structural Analysis, New York: McGraw-Hill, 1968.

23. Zienkiewicz, O. C., The Finite Element Method in Engineering Science, 3rd Edition, London: McGraw-Hill, 1977.

MONTANA STATE UNIVERSITY LIBRARIES
3 1762 10015329 3

THESIS

N378
R119
cop.2

Radons, Stephen W
Frequency response analysis of the in-vivo human spine

DATE	ISSUED TO

THESIS

N378
R119
cop. 2